2009-11-03

Investigate Correlations of Microstructures, Mechanical Properties and FSW Process Variables in Friction Stir Welded High Strength Low Alloy 65 Steel

Lingyun Wei
Brigham Young University - Provo

Investigating Correlations of Microstructures, Mechanical Properties and FSW Process Variables in Friction Stir Welded High Strength Low Alloy 65 Steel

Lingyun Wei

A dissertation submitted to the faculty of
Brigham Young University
in partial fulfillment of the requirements for the degree of

Doctor of Philosophy

Tracy W. Nelson, Chair
Brent L. Adams
Carl D. Sorensen
Mike P. Miles
Brian D. Jensen

Department of Mechanical Engineering

Brigham Young University

December 2009

ABSTRACT

Investigate Correlations of Microstructures, Mechanical Properties and

FSW Controlled Variables in Friction Stir Welded

High Strength Low Alloy 65 Steel

Lingyun Wei

Department of Mechanical Engineering

Doctor of Philosophy

The present study focuses on developing a relationship between process variables, mechanical properties and post weld microstructure in Friction Stir Welded HSLA 65 steel. Fully consolidated welds can be produced in HSLA 65 steel by PCBN Convex-Scrolled-Shoulder-Step-Spiral (CS4) tool over a wide range of parameters. Microstructures in the nugget center (NC) are dominated by lath bainite and a few polygonal/allotriomorphic grain boundary ferrites. FSW dependent variables are related to FSW independent variables by non-linear relationship. Heat input is identified to be the best parameter index to correlate with microstructures. With increasing heat input, the volume of bainite is reduced, the shape of bainite is more curved and grain/lath size become coarser. A linear relationship was established between heat input and semi-quantitative post-weld microstructures based on the optical microstructures.

Further analysis has been applied on the NC to obtain more fundamental understanding of FSW. The new approach via Orientation Imaging Microscopy (OIM) was developed to acquire quantitative microstructural data including bainite lath/packet and prior austenite grain size (PAG). A linear relationship between heat input and quantitative microstructural features in the NC have been established. Mechanical properties exhibits linear relationship with heat input. These correlations can be utilized to determine FSW weld parameter to get desired mechanical properties welds.

Keywords: Lingyun Wei, friction stir welding, high strength low alloy 65 steel, microstructures, bainite, prior austenite reconstruction, mechanical properties, controlled variables, quantitative grain size.

ACKNOWLEDGMENTS

I would like to thank all of those who have been influential while writing this dissertation. First, I would like to gratefully acknowledge the contributions of my advisor, Dr. Tracy W. Nelson for countless hours of guidance, direction and supervision throughout the project, as well as allowing me to learn and gain the confidence that I can accomplish great things; Second, Dr. Jeffrey Farrer for assistance with TEM, SEM and OIM operations.

Financial support for this work was provided by the Office of Naval Research, contract No. N00014-08-1-0025.

TABLE OF CONTENTS

LIST OF TABLE ..... **vii**

LIST OF FIGURES ..... **ixx**

1 Introduction **1**

1.1 Friction Stir Welding 1

1.2 Limitation of Previous Research 1

1.3 Objective 2

1.4 About this Dissertation 2

2 Correlations of Microstructures and Process Variables in FSW HSLA-65 Steel **3**

2.1 Introduction 3

2.2 Experiments 5

2.3 Results and Discussions 8

2.3.1 Relations between Independent and Dependant Variables in FSW 8

2.3.2 Comparison of FSW Parameter Indexes 10

2.3.3 Process Variables' Effects on Microstructures in Nugget Center (NC) 12

2.3.3.1 Microstructures in NC 12
2.3.3.2 Correlate Post-Weld Microstructures with Process Variables 17

2.4 Conclusions 20

3 Influence of Heat Input on Microstructural and Mechanical Properties of Friction Stir Welded HSLA-65 Steel **21**

3.1 Introduction 21

3.2 Experiments 24

3.3 A New Approach Developed to Acquire Quantitative Microstructural Data 27

3.3.1 Reconstruction of PAGs from Room Temperature Ferrite in the NC 27

3.3.2 A Quantitative Approach to Bainite Packet Size Measurement 33

3.3.3 Bainite Lath Size Measurement 35

3.4 Results and Discussions 36
3.4.1 Quantitative Data Collected by Using New Approaches 36
3.4.2 Heat Input Effects on Post-Weld Structures 37
3.4.2.1 Effect of Heat Input on Microstructures in the NC 37
3.4.2.2 Quantitative Microstructural Features in the NC 40
3.4.3 Effect of Heat Input on Mechanical Properties in the NC 41
3.5 Conclusions 43
References 45

LIST OF TABLES

Table 2-1: Measured chemical composition of HSLA-65 steel (wt. %) [16] .....…….5

Table 2-2: Average heat input value for each process parameter of HSLA-65 FSW, the bold parameters are selected to establish the correlations with post-weld microstructures .....…….8

Table 2-3: Semi-quantitative grain size in the NC with changing power and heat input .....……16

Table 3-1: Selected FSW process parameters with corresponding power and heat input .....……25

Table 3-2: Comparison of measurement taken by OIM™ and TEM .....……36

Table 3-3: Quantitative data of microstructures in the FSW NC.....……37

Table 3-4: Tensile properties and hardness in the FSW NC.....……42

LIST OF FIGURES

Figure 2-1: Grain structures of base metal 6

Figure 2-2: Geometry of CS4 tool used in the welding 7

Figure 2-3: PHI, APR, power and heat input versus FSW process parameters 11

Figure 2-4: Marco etched transverse cross section of FSW HSLA-65 weld, yellow square shows the nugget center (NC) 12

Figure 2-5: Microstructures of the weld nugget centre (NC) at various heat inputs, white square shows the curved bainite lath boundaries 14

Figure 2-6 Schematic diagram shows how the grain/lath measurement made. B represent bainite, α represent polygonal ferrite 16

Figure 2-7 Bainite lath size versus FSW process variables 17

Figure 2-8: Variation of heat input versus (a) grain Size (b) bainite lath size 18

Figure 2-9: Width of HAZ versus heat input 19

Figure 3-1: Cross section of a FSW weld in HSLA-65, yellow square shows the FSW nugget centre (NC). The sample was etched by 2% Nital 25

Figure 3-2: Schematic illustration for coordinate axes of pole figure (PF) 26

Figure 3-3: Location and dimensions of longitudinal tensile test samples 27

Figure 3-4: (a) Idea PF: stereographic plot of {001}α poles for K-S and N-W variants projected onto the (001)γ plane. Black and red dots represent K-S and N-W variants, respectively. Blue dots represent hypothetical austenite. [] (b) Ideal PF is rotated by 45° around RD,TD and ND 28

Figure 3-5: (a) IPF with IQ map shows NC microstructures. Black rectangle shows the cropped region (b) PF of the NC microstructures 29

Figure 3-6: PF of the region cropped (region in black rectangle) from Figure 3-5a 30

Figure 3-7: (a) Rotated PF of the cropped region. (b) Eliminated the outliers in rotated PF (c) Eliminated outliers in IQ map, the non-highlighted part is one prior austenite grain. (d) PF of the reconstructed prior austenite grain (after eliminating the outliers) 31

Figure 3-8: (a) IPF of the nugget center. (b) Reconstructed map of prior austenite grains in FSW nugget center, the number in the figure shows the individual austenite grains. The circle

shows the new method to measure the PAG size, where the white solid circles show the interception of the circle with the PAG boundary. 32

Figure 3-9: (a) IPF of the FSW NC, white space shows the irregular cropped region. (b) IQ map with the trace line across it. (c) Misorientation map is in red, high peaks show in black solid circles. IQ curve is in blue, red solid circles show the lower peak quantities. (d) PF, the variants are indicated by numbers.....34

Figure 3-10: Measurement of bainite packet and lath sizes are taken at multiple locations in the FSW NC.....36

Figure 3-11: (a)-(d) Microstructures of weld nugget centre (NC) at various heat inputs, (e) base metal (BM).....39

Figure 3-12: (a) Bainite lath size (b) bainite packet size (c) PAG size varies with changing heat input (d) bainite lath/packet size versus prior austenite grain size 41

Figure 3-13: (a) YS/UTS versus HI (b) YS versus bainite lath/packet sizes (c) Hall-Petch relations between YS and bainite lath/packet in the FSW NC 42

1 INTRODUCTION

1.1 Friction Stir Welding

Friction Stir Welding (FSW) is a solid state technology that has been attracting considerable interest since it was invented at TWI in 1991. FSW utilizes a non-consumable tool that is inserted into the abutting edges of the base metal. The rotating tool generates heat by friction between itself and the base plate, and induces plastic deformation in the weld zone to complete the joining process. [1]

FSW has shown distinct advantages over traditional arc welding. Because there is no melting, FSW produces less distortion, and defects associated with cooling from liquid phase are eliminated. [2] In addition, FSW is a "green technology" in that it produces no arc radiation, no fumes, and no hazardous waste.

1.2 Limitation of Previous Research

Previous research has demonstrated the feasibility of FSW HSLA type steels, all of which exhibited satisfactory mechanical properties. Some studies have shown limited analysis of post-weld microstructures of HSLA 65. Much of the work on microstructures is limited to single parameter weld. Previous studies were conducted without examining the effect of changing FSW parameters. The relationship between FSW input variables and machine outputs has not been investigated. In addition, they lack detailed quantitative analysis of post-weld

microstructures. As a result, correlations of microstructures, mechanical properties and FSW process variables have not been well-established.

1.3 Objective

The purpose of this study is to examine relationships between FSW process variables, evaluate the effects of a broad range of parameters on post-weld microstructures, determine the appropriate parameter index to correlate with microstructural evolution, and compare the effects of dependent and independent variables on post-weld microstructures. A new approach is developed to acquire quantitative microstructural data in FSW. Correlations are established between post-weld microstructures and heat input, grain size and mechanical properties. These correlations can be used to predict the mechanical properties and microstructures of the FSW weld.

1.4 About this Dissertation

This thesis consists of a collection of two papers that have been submitted for publication. The first paper qualitatively correlates between microstructures and process variables in FSW HSLA-65 Steel. The second paper quantitatively describes the influence of heat input on microstructural and mechanical Properties of Friction Stir Welded HSLA-65 Steel.

2 CORRELATIONS OF MICROSTRUCTURES AND PROCESS VARIABLES IN FSW HSLA-65 STEEL

2.1 Introduction

Friction Stir Welding (FSW) is a solid state joining process that can produce superior material properties to those produced by conventional welding methods. FSW can be used to join high-strength aluminum alloys that are difficult to weld by conventional arc welding. The intense plastic deformation produces a fine equiaxed microstructure due to dynamic recrystallization. [3,4,5] As-welded 7075Al-T651 shows a reduction in yield and ultimate strengths in the weld nugget which is associated with the coarsening of the very fine hardening precipitates. [3,4] Rapid implementation of FSW aluminum alloys into industry applications has motivated its application to other non-ferrous materials, such as Mg, [6] Ti, [7,8] and Cu. [9,10]

Although most FSW efforts have focused on aluminum alloys, there is considerable interest in the application of this technology to steels. Several studies have reported FSW of carbon and stainless steels. FSW of carbon and ultrafine grained plain low-carbon steels have shown increased strength in the stir zone due to refined microstructures and the formation of martensite and bainite. [11,12,13] FSW welded 304L stainless steel exhibited higher tensile properties than base metal. [14] FSW can refine the grains in stir zone of 2507 super duplex stainless steel which can maintain 50/50 austenite/ferrite in the weld. [15]

In recent years, there has been much interest in FSW of high strength low alloy (HSLA) type steel. HSLA type steels are relatively new structural steels for use in applications requiring

high strength, ductility and good weldability, such as ship building, oil and gas line pipe. HSLA steels are manufactured by Thermo-Mechanical Controlled Processing (TMCP), which produces uniform refined microstructures providing superior combination of high-strength and excellent toughness. [16] In conventional arc welding of HSLA steel, the heat affected zone (HAZ) is susceptible to hydrogen-assisted-cracking (HAC). Moreover, significant loss of strength and toughness in the HAZ can seriously compromise the mechanical properties of the weld. [16]

FSW has offered distinct advantages relative to the arc welding of HSLA type steels. Previous research demonstrate the feasibility of FSW HSLA 65 [17], X80 and L80 steels [18]; all of which exhibited satisfactory mechanical properties. Some studies have shown limited analysis of post-weld microstructures of HSLA 65 [19,20,21], X80 and L80 [18]. Softening of HAZ in HSLA 65 [21] and X80 [18] weldments were also reported. These previous studies were conducted without examining the effect of changing FSW parameters.

The influence of FSW parameters on the microstructure and mechanical properties were studied by a number of investigators on Al and Mg alloys. Querin [22] and Rodrigues [23] found higher rotation speed resulted in finer microstructure in FSW AA2219-T87 and AA6016-T4. Afrin [24] and Cao [25] reported larger grain size and decreasing tensile properties at lower welding speed in FSW AZ31B magnesium alloy. Cui [26] concluded the welding speed strongly affected the total size of stir zone of A356 cast alloy. Pilchak [27] showed the welding speed had an insignificant effect on grain size of FSW Ti-6Al-4V alloy.

Most research to date has tried to correlate FSW independent variables with post-weld properties. Research is limited on the investigation of the correlations between FSW dependent variables-power and heat input and post-weld characteristics. In tradition arc welding, it is common practice to correlate welding process parameters and microstructures with weld heat

input. Correlations between grain size in the HAZ/width of the HAZ and process parameters have been well established in traditional fusion welding. [28,29] Nelson [30] reported that peak temperatures in HAZ and microhardness increased with increasing heat input in FSW HSLA 65. However, the extent to which the dependent variables influenced the microstructural evolution of FSW HSLA 65 weld is yet unknown. No correlation between dependent variables and microstructures has been established.

The purpose of this study is to examine the relationship between FSW process variables, evaluate the effects of a broad range of parameters on post-weld microstructures, determine the appropriate parameter index to correlate with microstructural evolution, compare the effects of dependent and independent variables on post-weld microstructures and establish the correlations between the microstructures, and controlled variables of friction stir welded joints of HSLA 65 steel.

2.2 Experiments

The chemical composition of HSLA 65 (ASTM A945) used in the experiments is provided in Table 2-1. The base metal microstructure consists of refined upper bainite islands randomly embedded in the polygonal fine-grained ferrite matrix, with the average grain size about 8μm as shown in Figure 2-1.

Table 2-1: Measured chemical composition of HSLA-65 steel (wt. %) [16]

Element	*wt. %*	*Element*	*wt. %*
C	0.081	Cr	0.15
Mn	1.43	Cu	0.26
Si	0.2	N	0.009
S	0.003	V	0.055
P	0.022	Ti	0.013
Ni	0.35	Nb	0.021
Mo	0.063	Al	0.018
Fe	Balance	Boron	<0.0005

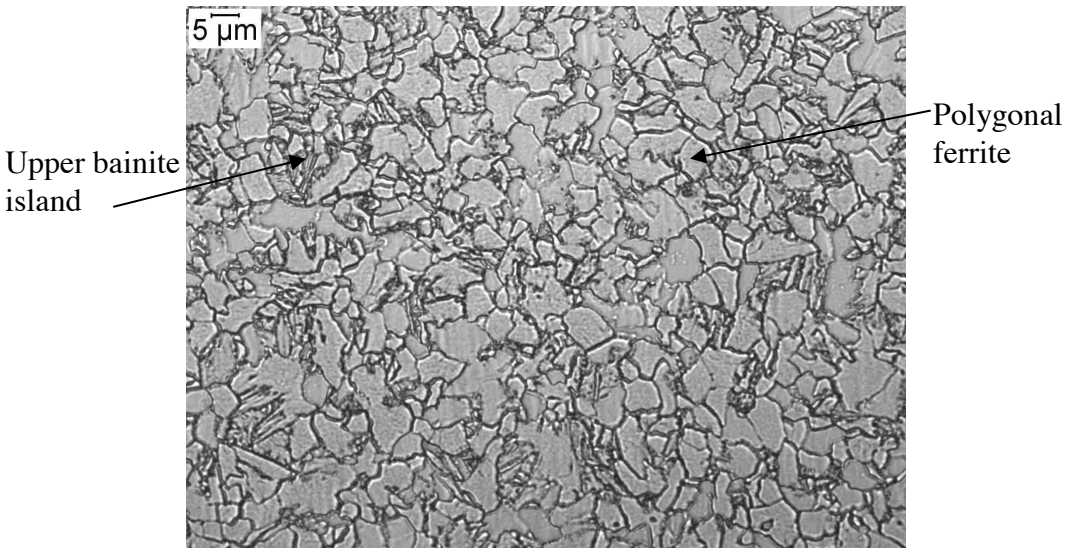

Figure 2-1: Grain structures of base metal

Test plates were prepared from 9.5mm (0.375 inch) thick rolled plate with dimensions of 762 mm (30 inches) in length and 203.2 mm (8 inches) in width. The long axis of the test plate was parallel to rolling direction. Each plate was lightly ground on both sides to remove oxide and surface scale prior to welding. Before welding, the plate was degreased with a methanol solvent. All welds were performed under a depth-controlled process. Partial penetration welds were made parallel to the plate rolling direction. Argon, at a flow rate of $1.1 m^3/h$, was used as shielding gas to protect both the tool and the weld area from surface oxidation.

A Convex-Scrolled-Shoulder-Step-Spiral (CS4) tool was used for all the welds. The shoulder and pin section of the tool are manufactured from solid PCBN (polycrystalline cubic boron nitride). The geometry of the CS4 tool is shown in Figure 2-2. 0.5º head tilt was applied during plunge and welding. All process parameters and torques were recorded during welding.

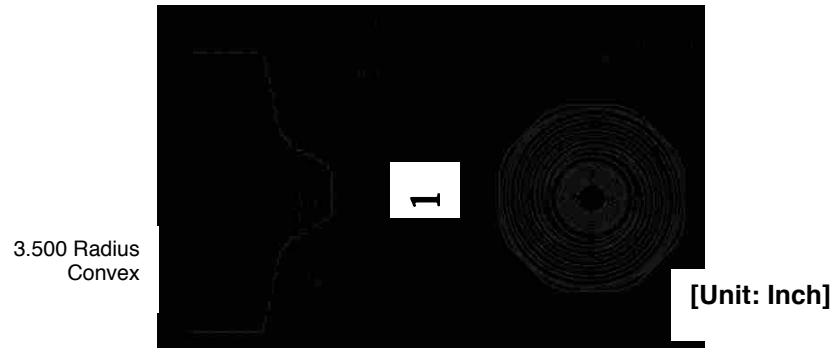

Figure 2-2: Geometry of CS4 tool used in the welding

Trial experiments were conducted to determine the working range of the rotation speed and welding speed. Feasible limits of the parameters were chosen to ensure that the friction stir welded joints were free from any defects. Fully consolidated welds were made at all selected parameters, which are summarized in Table 2-2. The corresponding axial-force and spindle torque are also shown in Table 2-2. The recorded spindle torque increases with increasing welding speed and decreasing rotation speed which is similar to that reported by Cui [26].

Equations (2-1) and (2-2) were used to calculate the power and heat input, as shown below,

$$P = \frac{(2\pi)\Omega T}{60} \tag{2-1}$$

$$H.I. = \frac{P.I.}{v} \tag{2-2}$$

Where P is power (KW); Ω is rotation speed (rpm); T is recorded torque by FSW machine (N.m); H.I is heat input (J/mm); and υ is welding speed (mm/min).

In order to establish correlations between post-weld microstructures and FSW process variables, four different welding parameters (shaded in yellow in Table 2-2) were chosen. The selected welding parameters covered the extreme and intermediate levels of power and heat

input, based on the data in Table 2-2. The selected parameters represent the widest range of power, heat input and independent variables.

Table 2-2: Average heat input value for each process parameter of HSLA-65 FSW, the bold parameters are selected to establish the correlations with post-weld microstructures

Rotation Speed (rpm)	*Welding Speed (mm/min)*	*Axial-Force (kg)*	*Spindle Torque (N.m)*	*Power (KW)*	*Heat Input (J/mm)*	*Advance per revolution (inch/rev)*	*Pseudo Heat Index (rev^2/inch)*
300	**51**	**3410**	**90**	**2.8**	**3329**	**0.006667**	**45000**
300	107	4297	119	3.8	1773	0.016667	18000
300	**203**	**4725**	**141**	**4.4**	**1308**	**0.026667**	**11250**
450	51	3144	71	3.3	3926	0.004444	101250
450	107	3769	85	4.1	1914	0.011111	40500
450	203	3740	98	4.6	1365	0.017778	25312.5
600	**51**	**3051**	**58**	**3.6**	**4272**	**0.003333**	**180000**
600	107	4970	76	4.8	2253	0.008333	72000
600	**203**	**3956**	**85**	**5.4**	**1583**	**0.013333**	**45000**

Transverse samples were removed from the welds for optical metallography analysis. Each sample was ground and polished successfully through 1μm diamond paste. Samples were etched with 2% Nital and analyzed optically at magnification up to 1000X using an Olympus GX51 microscope.

2.3 Results and Discussions

2.3.1 Relations between Independent and Dependant Variables in FSW

In order to correlate post-weld microstructures with process variables, it is necessary to understand the relationship between FSW independent and dependent variables. In traditional arc welding, those relations have been well-established. Power and heat input are controlled by independent variables: welding current, voltage and travel speed. Power and heat input have a linear relationship with these independent variables, e.g. increase with increasing welding

voltage and current, and deceasing welding speed. They can be controlled directly by variation of arc current and voltage. [28]

FSW is substantially different from arc welding. The independent variables in FSW include rotation speed, welding speed, axial-force, tool geometry and tool material. These variables can be directly controlled by the operator. The dependent variables are heat input, power and spindle torque. Unlike arc welding, power and heat input in FSW cannot be controlled directly by independent variables. Power is dependent on rotation speed and spindle torque. Spindle torque is not a controlled variable, rather a response variable. [31] To complicate matters, spindle torque is a function of rotation speed, welding speed, tool geometry, tool material and tool depth/axial-force. Thus, it is difficult to develop simple relationships between independent and dependent variables.

Early FSW machines did not have the ability to monitor or record spindle torque. As a result, earlier researchers attempted to establish simple empirical relationships between input variables and machine outputs. Pseudo Heat Index [32,33,34] and Advance per Revolution [31] were developed as parameter indexes to correlate with peak temperature and mechanical properties in the weld. PHI and APR are defined in Equation (2-3) and (2-4).

$$PHI = \frac{rpm^2}{ipm} \tag{2-3}$$

$$APR = \frac{ipm}{rpm} \tag{2-4}$$

Where rpm is rotation speed (revolution per minute), ipm is welding speed (inches per minute).

From the definitions of PHI and APR, these indices do not take into account the effect of spindle torque or capture the specific energy of the process. Since post-weld microstructures strongly depend on heat input, which is well-established in traditional arc welding, [28,29] it is

critical to capture the effect of the specific energy within the FSW parameter index. Therefore, it is likely that power and heat input will exhibit better correlation with post-weld microstructures. The comparison of those parameters indices in Section 2.3.3.2 will provide addition evidence to identify the best process variable to correlate with microstructures.

2.3.2 Comparison of FSW Parameter Indexes

In order to demonstrate the characteristics of PHI, APR, P (power) and HI (heat input), comparisons of these parameter indexes are discussed in this section. Using the data in Table 2-2, PHI, APR, power and heat input are plotted versus FSW rotation speed and welding speed. These three dimensional plots are shown in Figure 2-3.

PHI exhibits a second order linear relationship with rotation speed and reciprocal relationship with welding speed as shown in Figure 2-3a. APR exhibits linear relationship with welding speed, but displays reciprocal relationship with rotation speed as shown in Figure 2-3b. The comparison generalizes APR is less complicated parameter index, since it has lower order relationship than PHI.

PHI and APR both have redundancies at different parameters which exhibit poor correlations with microstructures. The redundancy prevents an accurate correlation between parameters and microstructural features. As observed in Figure 2-3a, 600rpm/203mm/min and 300rpm/51mm/min have the same PHI values, but these two parameters have different power and heat input. In addition, although there is no redundancy shown in the APR plot, APR still has the possibility to have redundancy at different FSW independent variables. For example, 600rpm & 8ipm has the same APR value with 300rpm & 4ipm, but they have different heat input. The redundancy in PHI and APR make it difficult to establish accurate correlations because they do not capture the effect of specific energy, peak temperature and cooling rate.

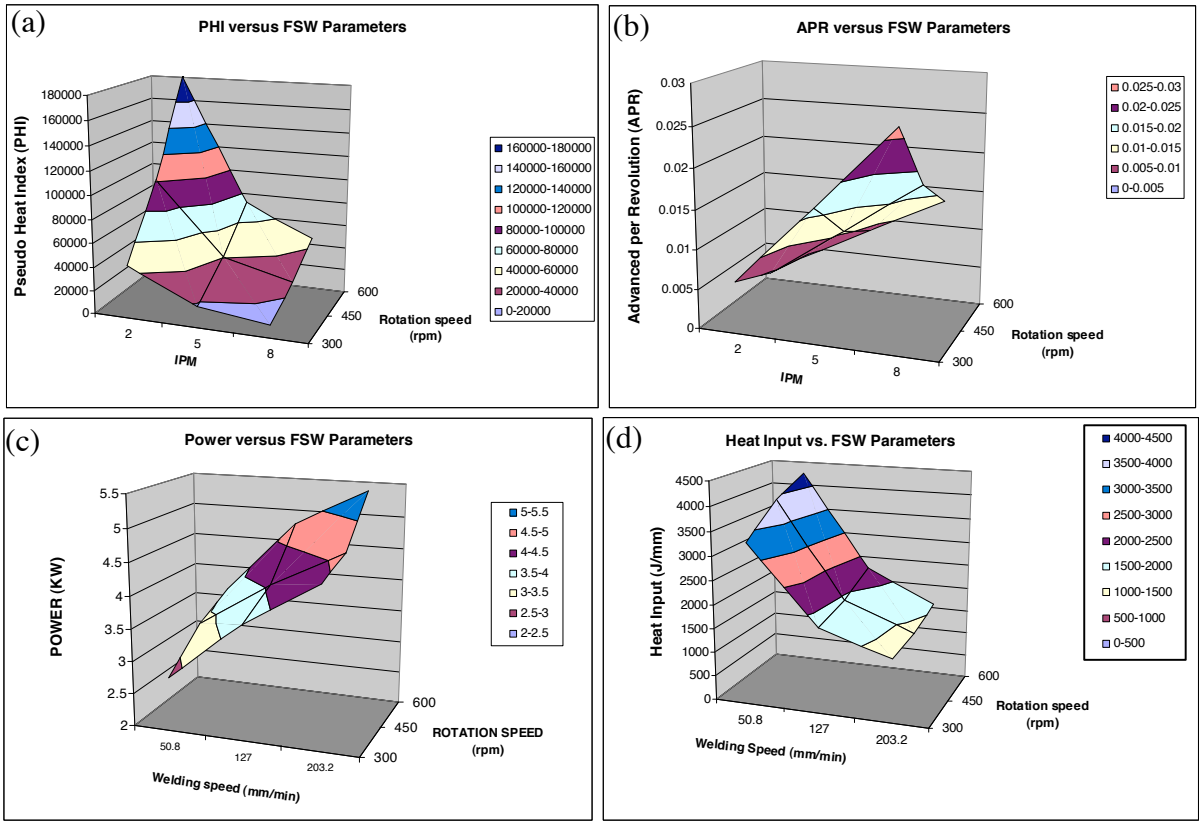

Figure 2-3: PHI, APR, power and heat input versus FSW process parameters

Power and heat input display non-linear relationships with rotation speed and welding speed, as shown in Figure 2-3c and d. This is similar to the report by Pew [35] in FSW Al Alloys 7075, 5083 and 2024. The non-linear relationships are because power and heat input are the function of spindle torque, and spindle torque as discussed earlier is a response variable. So single or two parameters are inadequate to analyze the non-linear relationship. In this study, four parameters were chosen to establish the correlation with the microstructural characteristics of FSW HSLA 65 over a broad range of parameters. (Shown in Table 2-2)

2.3.3 Process Variables' Effects on Microstructures in Nugget Center (NC)

2.3.3.1 Microstructures in NC

In this section, some consideration will be given to post-weld microstructural changes in FSW weld nugget at different heat inputs. The nugget center (NC) shown in Figure 2-4, is the position used for comparison between weld parameters. The NC is distinguished by the region at the vertical centerline of the stir zone which has equal distances to the top surface and bottom of HAZ in the weld.

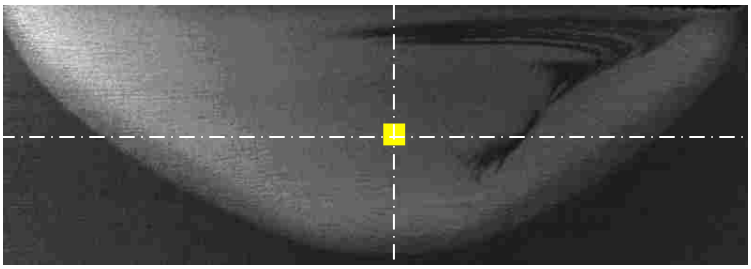

Figure 2-4: Marco etched transverse cross section of FSW HSLA-65 weld, yellow square shows the nugget center (NC)

Figure 2-5 compares the microstructural features within the NC at various heat inputs. The tool rotation speed (rpm) and welding speed (mm/min) are noted in the upper right hand corner of each micrograph. Heat inputs are noted in the bottom left-hand corners. The symbols in these images represent different transformation products: α represents polygonal ferrite; α_{gb} represents grain boundary allotriomorphic ferrite; B represents bainite; and α_w represents Widmanstätten ferrite. From these optical images, several microstructural characteristics can be observed.

There is no evidence of base metal (BM) microstructures in Figure 2-5. The equiaxed grains in BM have completely transformed to lath bainite with some polygonal/grain boundary

ferrite. This indicates the BM has reached a peak temperature in excess of the A_3, even at the lowest heat input 1308J/mm.

It is well known that microstructural changes are strongly dependent on peak temperature and subsequent cooling. Cooling rate is associated with heat input, i.e. lower heat input produces faster cooling rate. [36] At the lowest heat input in Figure 2-5a, the microstructure is mainly lath bainite. The bainite structure consists of lath ferrite with discontinuous carbide particles at the lath boundaries: typical of upper bainite morphology. The lath boundaries are relative straight and parallel.

With increasing heat input, two kinds of microstructures are formed (shown in Figure 2-5b-c): polygonal ferrite and upper bainite. That is because higher heat input produces slower cooling rate, equiaxed polygonal ferrite starts to nucleate at ferrite/austenite boundaries and extend into untransformed austenite grain interiors. [37] In addition, some bainite lath boundaries have more curvature as marked in square in Figure 2-5c. That may be due to higher heat input which induces higher peak temperature causing the base metal to be deformed more easily than at lower heat input.

In Figure 2-5d, at the highest heat input 4270J/mm, the primary microstructures are lath bainite along with dispersed particles at prior austenite grain boundaries coexisting with some polygonal and allotriomorphic grain boundary ferrite. Allotriomorphic ferrite forms at a triple junction of prior austenite grain boundaries. [37] Long needle shape Widmanstätten ferrite is observed in Figure 2-5d. This has been also reported by Pao [20] in stir zone of FSW HSLA-65.

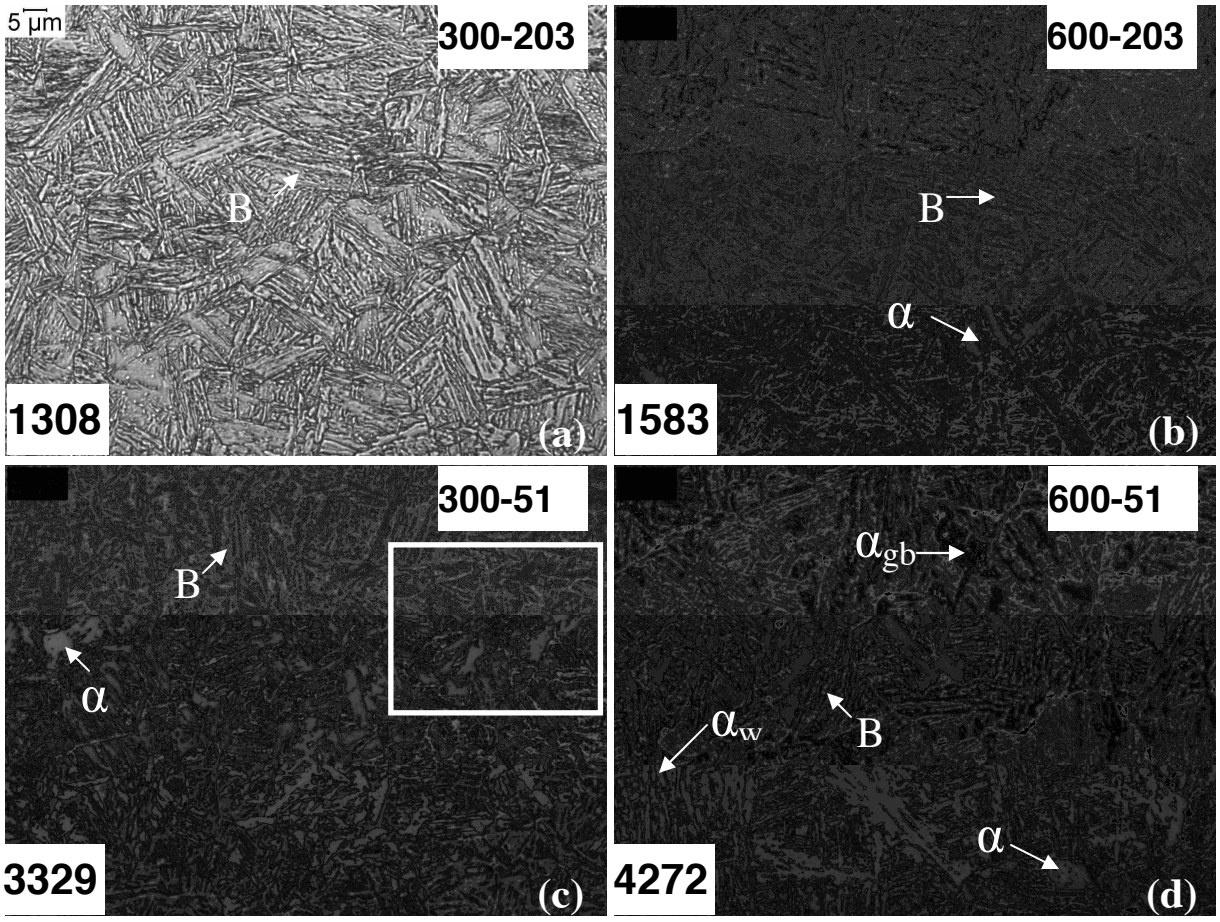

Figure 2-5: Microstructures of the weld nugget centre (NC) at various heat inputs, white square shows the curved bainite lath boundaries

In summary, with increasing heat input, the volume fraction of bainite decreases, while the volume fraction of polygonal/allotriomorphic grain boundary ferrite increases. In addition, bainite lath boundaries are straighter at lower heat input and have more curvature at higher heat input. Although higher temperature transformation products-(polygonal and allotriomorphic grain boundary ferrite) are formed at higher heat input, lath bainite is still the dominated microstructure in the FSW NC. This is due to the relatively fast cooling rate in FSW compared to arc welding since the weld plate is clamped tightly to the anvil creating greater heat conduction.

Prior austenite grains (PAGs) are also visible in these figures. However, most of the grain boundaries appear to be discontinuous. This is due to the interaction of the etchant used and the HSLA type steel. The etchant is unable to attack the grain boundaries (GBs) sufficiently due to the small amount of alloys at GBs. Despite this, the PAG size appears to increase with the increasing heat input.

In order to investigate correlations between microstructures in the NC and FSW process variables, grain/lath size measurement are needed. Since the prior austenite grain boundaries are absent for the most part, any assessment of PAGs size from optical images would be strictly qualitative. In addition, the bainite lath size is also difficult to quantify by optical microscopy even at higher magnification-1000x because bainite lath structure is very fine. Therefore, grain/lath size in the FSW NC are estimated approximately based on optical images.

Figure 2-6 illustrates how the grain/lath measurements are made to acquire semi-quantitative data. Discontinuous PAG boundaries are highlighted by white curved lines in this figure. PAG is identified by the existing boundaries with some estimation. Bainite lath is measured by drawing a trace line (in black) perpendicular to lath boundaries, and counting the numbers (N) of the laths along this trace line. The true line length of the trace line is then measured and then divided by the laths number N. Polygonal ferrite grains are easily to identify as shown in this figure too. The grain sizes of ferrite and PAG are measured by using a new method developed in this study. The detail procedures of the new method are described in Section 3.4.

The average grain/lath sizes are shown in Table 2-3. The PAG grain size ranges from about 25μm to 65μm as heat input increases from lowest to highest heat input. Over this same range, bainite lath size increases from 0.9μm to 2.25μm. The authors believe the bainite laths

observed in these images consist of several thinner laths which are difficult to distinguish by optical microscope. The estimated lath sizes are likely larger than the actual value. This is demonstrated by the quantitative microstructural analysis in Section 3.4.1, which shows bainite lath size as fine as 0.653μm at lowest heat input 1308J/mm.

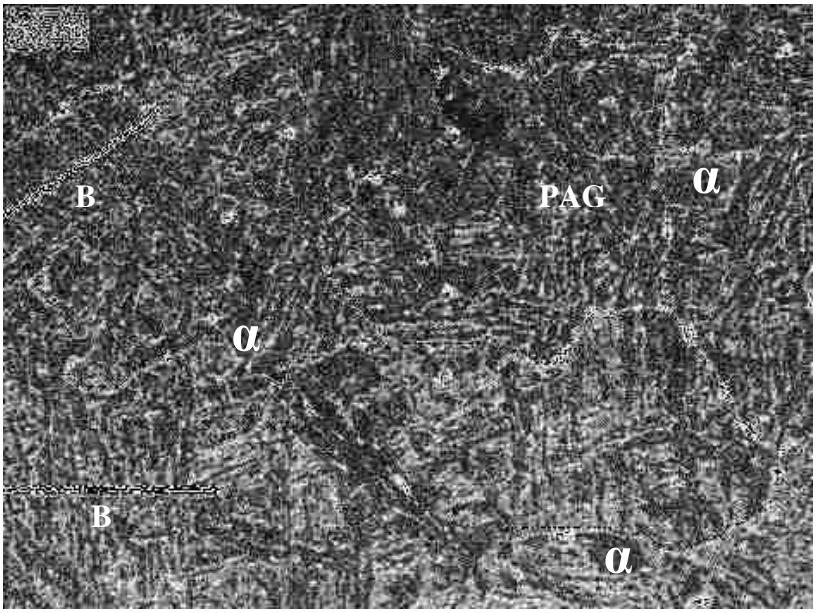

Figure 2-6 Schematic diagram shows how the grain/lath measurement made. B represent bainite, α represent polygonal ferrite

Table 2-3: Semi-quantitative grain size in the NC with changing power and heat input

PHI	*APR*	*Power (KW)*	*Heat Input (J/mm)*	*Bainite Lath (μm)*	*PAGs (μm)*	*Ferrite Grain Size (μm)*	*Width of HAZ (mm)*
11250	0.027	4.4	1308	0.9	25	10	0.14
45000	0.013	5.4	1583	1.25	30	12.5	0.26
45000	0.007	2.8	3329	1.5	40	13	0.35
180000	0.003	3.6	4272	2.25	65	25	0.50

2.3.3.2 Correlate Post-Weld Microstructures with Process Variables

In this section, correlations of the process variables with post-weld microstructures in the NC are investigated. Based on the data in Table 2-3, the bainite lath size is plotted against PHI, APR, PI and HI to identify the best process variable to correlate with microstructures.

In Figure 2-7, PHI plot displays redundancy where same PHI values have different bainite. In addition, PI does not exhibit consistent trend with increasing bainite lath. Although APR shows decreasing trend with increasing bainite lath measurement, it shows opposite consistent trend to traditional relationship, such as increasing grain/lath size with increasing heat input. Therefore, these indicate PHI, APR and PI have a weak correlation with the post-weld microstructures. Heat input is the best FSW process variable to correlate with post-weld microstructure in the weld nugget center (NC).

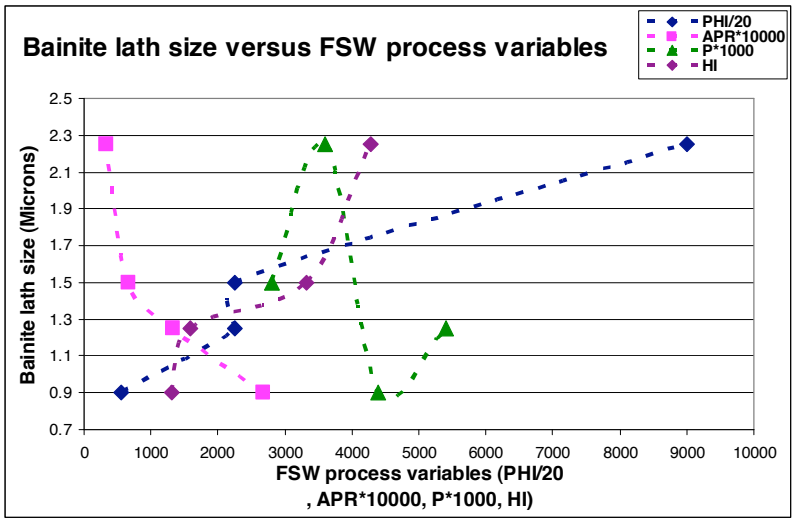

Figure 2-7 Bainite lath size versus FSW process variables

Using the data in Table 2-3, bainite lath size, ferrite grain and PAGs size are plotted against FSW heat input, shown in Figure 2-8. Figure 2-8(a) and (b) show the bainite lath, ferrite

and prior austenite grain size all increase with increasing heat inputs. Grain/lath sizes exhibits linear relationships with increasing heat input. The R^2 values shown in the plots indicate a good fit.

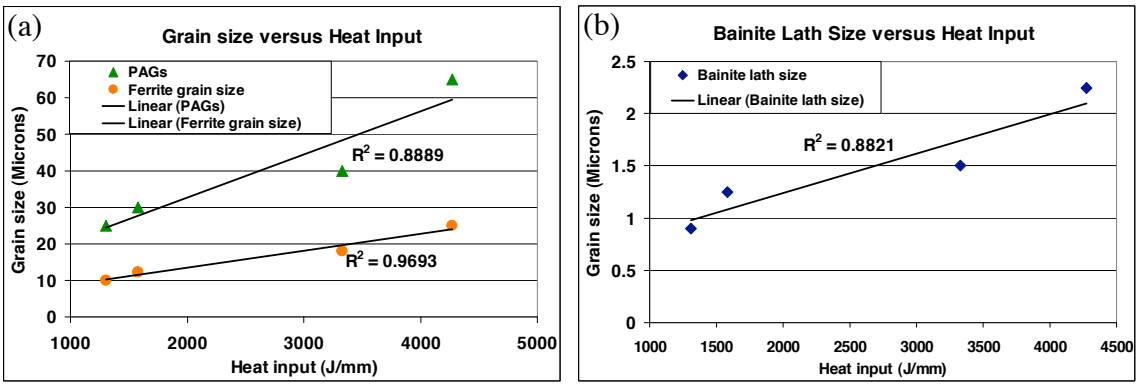

Figure 2-8: Variation of heat input versus (a) grain Size (b) bainite lath size

The width of the HAZ in FSW weld provides additional evidence of heat input dependence. The width measurement of the HAZ is obtained from Vickers hardness map of the weld, where the area with hardness less than 200Hv indicates the HAZ. In traditional arc welding, the width of the HAZ usually increases with increasing heat input. [28,29] In this study, the similar trend is found and shown in Figure 2-9, i.e., increasing width of the HAZ width is associated with increasing heat input in FSW welds. The width of the HAZ exhibits linear relationship with heat input. It demonstrates that weld properties in FSW is strongly correlated to heat input.

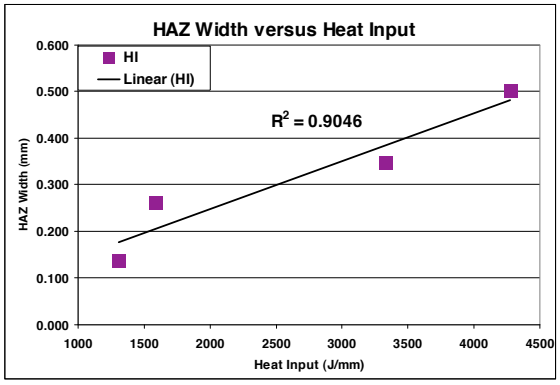

Figure 2-9: Width of HAZ versus heat input

The linear relationship between PAGs and heat input demonstrates peak temperature in the NC is dependent on heat input too. That is because longer dwell time and higher peak temperature in the austenite transformation zone will produce larger PAGs, but peak temperature is the dominant factor. [38] This is contrary to that reported by Reynolds [31]. Reynolds found peak temperature increases monotonically with increasing power in FSW 7050-T7451. The different results are because spindle torque was fixed in input torque FEM simulation model [39] to calculate peak temperature in Reynolds' paper. As a matter of fact, spindle torque is an output or response parameter which cannot be directly controlled by the operators as discussed in Section 2.3.1.

Strong correlation is established between heat input and FSW post-weld microstructures. Since peak temperature and cooling rate are governed by heat input in the FSW weld nugget center, higher heat input induces higher peak temperature or longer dwell time above A_3 in the NC, and also produces slower cooling rate. Peak temperature strongly affects prior austenite grain size. This produces coarser prior austenite grains. Coarser PAGs would transform to coarser microstructures at the same cooling rate since coarser PAGs provide fewer nucleation

sites at grain boundaries. [38] This combined with slower cooling rate prompt the formation of larger grain/lath structures with increasing heat input.

In the present study, linear correlations between heat input and post-weld microstructures in the FSW nugget center (NC) are established. Although they show a good fit, the accuracy is still in question since the microstructural data are acquired based on the optical images. The accuracy could likely be improved if the quantitative microstructural measurements are obtained. And the better correlations can be established between heat input and weld properties. Therefore, the new approach has been developed to acquire quantitative microstructural data and investigate their correlations to heat input in Chapter 3.

2.4 Conclusions

The following conclusions can be made from this investigation:

- Heat input is the best process variable to correlate with post-weld microstructures since it captures the effect of the specific energy of the FSW process.
- Grain/lath size in the NC increases with increasing heat input. The linear correlation between semi-quantitative post-weld microstructures and heat input is established.

3 INFLUENCE OF HEAT INPUT ON MICROSTRUCTURAL AND MECHANICAL PROPERTIES OF FRICTION STIR WELDED HSLA-65 STEEL

3.1 Introduction

Friction Stir Welding (FSW) is a solid state technology which utilizes a non-consumable tool that is inserted into the abutting edges of the base metal. The rotating tool generates heat by friction between itself and the base plate, and induces plastic deformation in the weld zone to complete the joining process. [1] Since it was invented by TWI in 1991, FSW has been successfully applied to various types of Al [3-5], Mg [6], Ti [7, 8], Cu [9, 10], carbon steels [11-13] and stainless steels [14, 15].

In recent years, there has been increasing interest to extend this technology to joining of high strength low alloy (HSLA) steel. HSLA type steels are relatively new structural steel for use in applications requiring high strength, ductility and good weldability such as ship building, oil and gas line pipe. HSLA steels are manufactured by Thermo-mechanical Controlled Process (TMCP) which produces uniform refined microstructures providing superior combination of high-strength and excellent toughness. [16]

FSW has attracted great attention in the industrial world due to its many advantages over arc welding in joining HSLA type steels. Since base material does not melt, FSW produces wrought instead of casting structure weld which has less distortion and metallurgical changes. In addition, the solid state process eliminates porosity and cracking in weld.

Previous research has demonstrated feasibility of FSW in joining HSLA 65 [17], X80 and L80 steels [18]. The post-weld structures exhibited satisfactory mechanical properties. Some of the studies focus on properties of single parameter welds. There have shown limited analysis on post-weld microstructures of HSLA 65 [19-21,40], X80 and L80 [18]. The stir zone of FSW HSLA 65 exhibits upper bainite and some polygonal/allotriomorphic ferrite structures. [19, 20] Softening of HAZ in HSLA 65 [21] and X80 [18] weldments were reported.

Some researchers have studied the influences of FSW controlled variables on post-weld microstructure in HSLA 65 steel. [41] The correlation between FSW heat input and microstructures in stir zone was developed. The paper reported the grain/lath size in weld nugget was highly dependent on heat input. A linear correlation between them was established. However, the microstructural analysis in this study was very qualitative.

It is known that mechanical properties of the welds in HSLA type steels highly depended on grain size. In traditional arc welding, good quantitative correlations of grain size in HAZ and width/area of HAZ with heat input, as well as tensile properties with grain size in HAZ have been developed. [28,29,42] Quantitative analysis in FSW is far behind the tradition arc welding. No well-established correlations between grain size and heat input, as well as grain size and mechanical properties in FSW HSLA 65 stir zone have been reported yet.

Quantitative microstructural data is essential to study these correlations and develop a more fundamental understanding of FSW. Bainite lath and packet size, and prior austenite grain size in the FSW stir zone are the primary factors affecting the post-weld properties. Previous research has not reported any quantitative analysis on FSW HSLA-65. The absence of quantitative microstructural data is due to the difficulty in acquiring such data. This is especially true in HSLA type steel which undergoes an allotropic transformation.

Because of the extremely fine structure of bainite, TEM is the primary approach applied to study bainite and measure the lath size. [43-46] Bainite packets are composed of low-misorientation-grain-boundary laths which have a similar common crystallographic orientation. [44] Two approaches have been used to analyze bainite packet-traditional etching and TEM. [45,46] However, TEM provides measurement of only very small area, so limited statistical data can be readily obtained. So lath/packet size measured by TEM may not represent the primary characteristics of the bainite structure.

Prior austenite grains (PAGs) in steels has been investigated by numbers of researches. [43,45,48,49] Traditional etching is usually used to reveal the prior austenite grain boundary. [45] This proved to work well to bring out PAG boundaries in high alloys steels. However, it is difficult to reveal PAG in low alloy steel such as HSLA type steel, since there are not many alloys precipitated at grain boundary to attack and bring out by etchant. As a result, PAG boundaries are discontinues at most parts in HSLA 65 steel. [41,47]

Some researchers have developed methods to reconstruct PAGs from room temperature ferrite/martensite by using EBSD data. Decocker [48] published an algorithm to identify all possible type of grain boundaries between product orientation of the same parent grain for Bain and K-S relations. Cayron [49] developed an approach based on the theoretical groupoid structure formed by the variants and their operators, and reconstructed PAG assuming a NW orientation only. Lambert-Perlade [43] presented a method to calculate orientation of PAG from K-S and N-W relations.

In the present study, OIM™ is used to acquire quantitative microstructural data in FSW. The objectives of this research are to develop the correlations between post-weld microstructures and heat input, grain size and mechanical properties. As these correlations can be well-

established, they can be used to determine FSW weld parameters for desired mechanical properties welds.

3.2 Experiments

The base material used in this investigation is 6.45mm-thick HSLA-65 steel (ASTM A945) with 450MPa (65ksi) and 538MPa (78ksi) minimum yield and ultimate strength, respectively. The average hardness of base metal is 200Hv. A nominal composition consists of Fe-1.43Mn-0.35Ni-0.063Mo-0.15Cr-0.26Cu-0.055V-0.013Ti-0.021Nb-0.081C (wt.%). Test plates were prepared from 9.5mm (0.375 inch) thick rolled plate with dimensions of 762 mm (30 inches) in length and 203.2 mm (8 inches) in width. The long axis of the test plate was parallel to rolling direction. Each plate was lightly ground on both sides to remove oxide and surface scale prior to welding. Before welding, the plate was degreased with a methanol solvent.

Partial penetration bead on plate welds were made in this investigation. All welds were performed under a position-controlled process. Argon atmosphere at a flow rate of 1.1m^3/h is introduced as shielding gas to protect both the tool and weld area from surface oxidation. The welding direction is parallel to the plate rolling direction and the weld penetrated through the normal direction of the plate. Welding of HSLA-65 was performed using PCBN (polycrystalline cubic boron nitride) Convex-Scrolled-Shoulder-Step-Spiral (CS4) tool. 0.5º head tilt was applied during plunge and welding. Four FSW parameters investigated are shown in Table 3-1 with corresponding power and heat input.

Table 3-1: Selected FSW process parameters with corresponding power and heat input

Group	*Rotational Speed (rpm)*	*Travel Speed (mm/min)*	*Power (KW)*	*Heat Input (J/mm)*
I	300	203.2	4.4	1312
II	450	203.2	4.6	1369
III	450	127	4.1	1919
IV	450	50.8	3.3	3936

Transverse metallographic samples were removed from each weld with a water-jet cutter. Samples were mounted in Bakelite then ground and polished successively through 0.05µm. EBSD data was acquired by using an FEI XL-30 SFEG operated at 25Kv. The scan step size was 0.2µm. OIM™ scans were performed on the FSW nugget center (NC) illustrated as the solid square in Figure 3-1. The NC is distinguished by the intersection region of the vertical and horizontal centerline in friction stir weld.

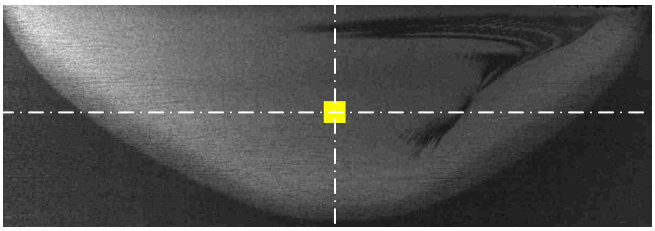

Figure 3-1: Cross section of a FSW weld in HSLA-65, yellow square shows the FSW nugget centre (NC). The sample was etched by 2% Nital

OIM data were acquired and analyzed in TSL 5.2 analysis software. The acquired data are rotated -90º about TD (Transverse Direction) to bring the principal axes of the crystal into coincidence with the principle axes of the process. Crystallographic data are expressed as inverse pole figure (IPF) maps, image quality (IQ) maps and {001} pole figures (PF). Coordinate axes of the pole figure are the RD, TD and ND as shown in Figure 3-2.

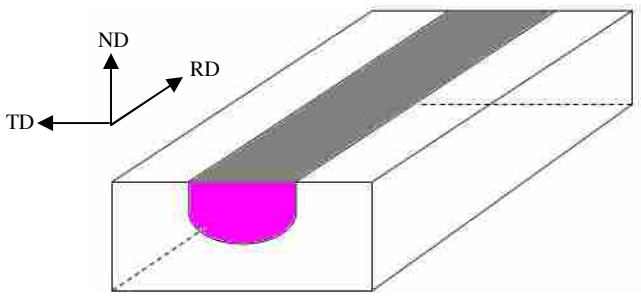

Figure 3-2: Schematic illustration for coordinate axes of pole figure (PF)

TEM foils were removed from the same location as shown in Figure 3-1. Transverse samples were prepared, and 3mm diameter cylinders were electrical-discharge machined (EDM) from the region of interest. 300μm thick discs are sliced by EDM from these cylinders for TEM analysis. The slices are thinned to 70μm for perforation by twin-jet electro-polishing using a solution of 10 vol. pct. Perchloric acid and 90 vol. pct. glacial acetic acid with 25V at room temperature. Microstructural investigation is carried out on a Philips Tecnai F30 TEM FEG instrument operated at 300 kV.

Hardness scans were made on the weld and surrounding base metal using a LECO LM 100AT microhardness tester. Using a Diamond Pyramid indenter, testing was performed using 300 gram applied load and 8 second dwell time. Indents were spaced at 300μm x 600μm. Average hardness in NC was acquired by measuring the hardness in the area of 3mm x 3mm in NC as shown in Figure 3-1. Width of HAZ is measured on mid-thickness hardness curve. HAZ is identified by the softening area compared with base metal. A line at 200Hv is drawn on mid-thickness hardness curve; the intercepted distance is the width of HAZ.

Longitudinal through-thickness tensile test were performed. Three 1mm-thick samples are removed from the FSW nugget center (NC) by EDM as shown in Figure 3-3, the middle sample was used to investigate tensile properties of the FSW nugget center and correlate with

post-weld microstructures. The tensile test was run at a crosshead speed of 0.762 mm/min by an Instron Model 123 test machine. Yield & ultimate tensile strengths were determined.

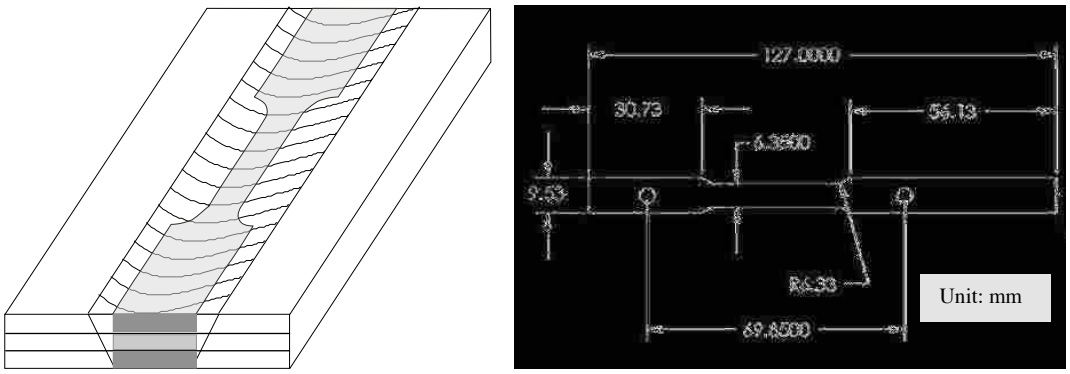

Figure 3-3: Location and dimensions of longitudinal tensile test samples

3.3 A New Approach Developed to Acquire Quantitative Microstructural Data

3.3.1 Reconstruction of PAGs from Room Temperature Ferrite in the NC

During a phase transformation, a specific orientation relationship usually exists between initial phase and the transformed product phase. For instance, bainite transforming from prior austenite has distinct Kurdjumov-Sachs (K-S) $\{111\}\gamma\langle 110\rangle\gamma // \{110\}\alpha\langle 111\rangle\alpha$ and/or Nishiyama-Wasserman (N-W) $\{111\}\gamma\langle 112\rangle\gamma // \{110\}\alpha\langle 110\rangle\alpha$ relationships. Because of the symmetry of the crystals, a single prior austenite orientation transforms to a number of final orientations called crystallographic variants. [50] The numbers of minimum angle-axis variants for K-S and N-W are 24 and 12, respectively. [51] If the coordinate system of the initial crystal is taken as the reference system, the pole figure representation of these two classical γ-to-α transformation relationships is shown in Figure 3-4a, where the {100} poles of the product phase (red and black) are projected onto the parent austenite (001)[100] (blue).

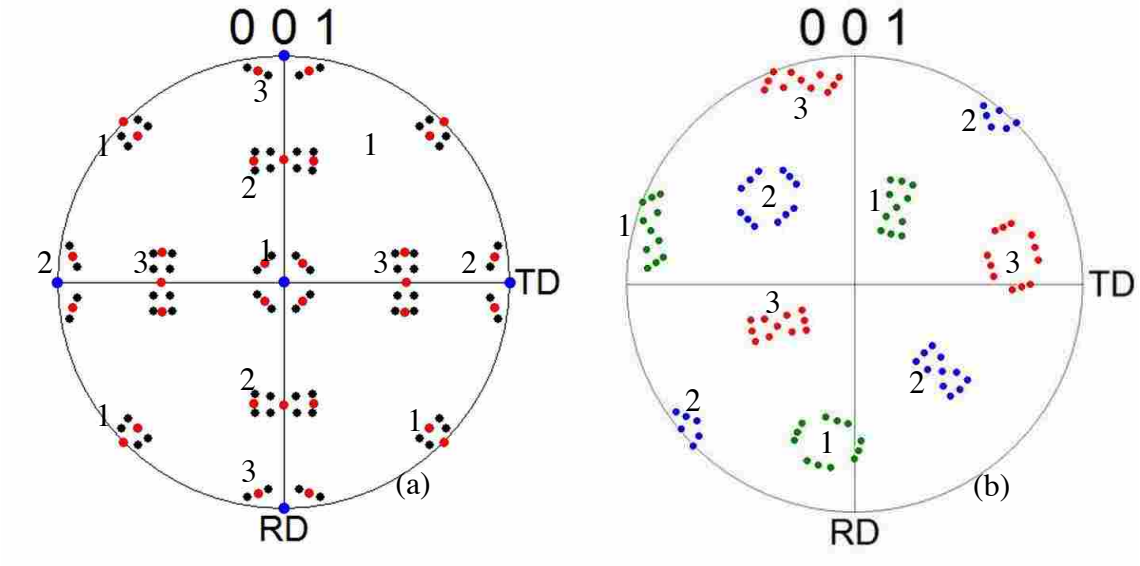

Figure 3-4: (a) Idea PF: stereographic plot of {001}α poles for K-S and N-W variants projected onto the (001)γ plane. Black and red dots represent K-S and N-W variants, respectively. Blue dots represent hypothetical austenite. [51] (b) Ideal PF is rotated by 45° around RD,TD and ND

In Figure 3-4a, there are three primary Bain zones represented by small truncated squares centered on the austenite <100> pole. [52] The three Bain zones are indicated by numbers 1 to 3. The K-S and N-W variants are symmetrically distributed about the Bain zone: eight K-S (blue) and four N-W (red) variants around each zone. Two bars associated with each Bain zone are located at the <110> poles in the stereographic plot, which are 45° away from <100> pole.

Figure 3-4a is designated as the ideal pole figure in this investigation. The ideal pole figure shows a maximum of 24 K-S and 12 N-W variants transformed from a hypothetical austenite (001)[100] due to the particular crystallographic orientation between austenite and bainitic ferrite. In order to better illustrate the primary Bain zones and associated bars, the ideal PF is rotated by 45° around RD, TD and ND as shown in Figure 3-4b. The three truncated Bain zones are clearly visible in this figure.

Since the ideal distribution of the bainite orientations from a given austenite grain is known, the orientation of the initial parent austenite grain can be determined. An example below shows the approach to reconstruction process.

An inverse pole figure (IPF) map and pole figure (PF) of FSW nugget center are obtained using EBSD as shown in Figure 3-5. From PF shown in Figure 3-5b, it is difficult to identify the primary Bain zones due to the large data set included. Therefore, smaller regions are cropped to reduce the data based on the prior austenite grain size.

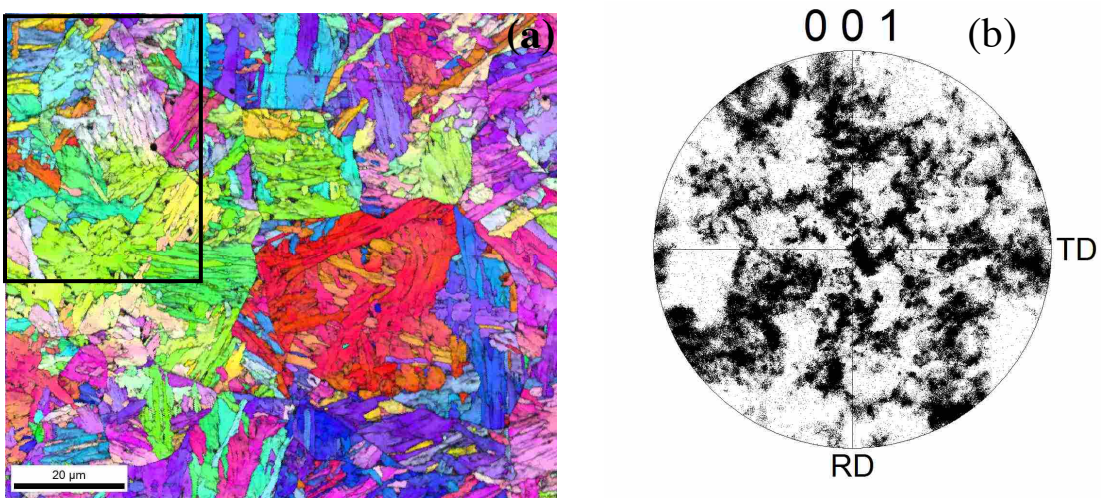

Figure 3-5: (a) IPF with IQ map shows NC microstructures. Black rectangle shows the cropped region (b) PF of the NC microstructures

Figure 3-6 shows PF of small region cropped from Figure 3-5a. In this pole figure, three primary Bain zones can be identified (circled in red). However, the bars associated with each Bain zone are not clearly visible. To facilitate the analysis, the data is rotated manually to match the ideal PF.

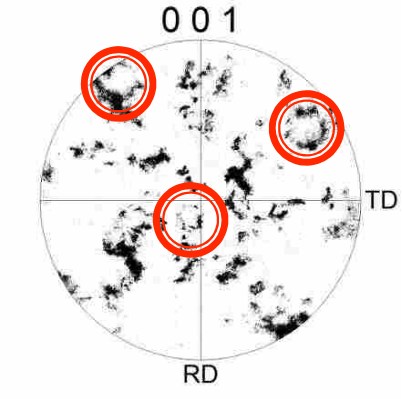

Figure 3-6: PF of the region cropped (region in black rectangle) from Figure 3-5a

The rotated pole figure is shown in Figure 3-7a. The three primary Bain zones are centered on $\{001\}_{\gamma}$. By comparing it with the ideal PF in Figure 3-4a, it is easy to identify the Bain zones and the outliers. The outliers that do not fall within the ideal PF are eliminated. They are highlighted in Figure 3-7b. In IQ map, the grains associated with those outliners are highlighted to display the grain boundary of the prior austenite grain. Figure 3-7c (non-highlighted part) shows the acquired reconstructed prior austenite grain.

The pole figure (PF) of the acquired PAG is shown in Figure 3-7d after the outliners (highlighted parts) have been removed. The primary Bain zones and associated bars are clearly visible. The bainite orientation relationship is well within the Bain zone. This illustrates that only one prior austenite grain exists. A few outliners are still observed which may come from grain boundary allotriomorphy.

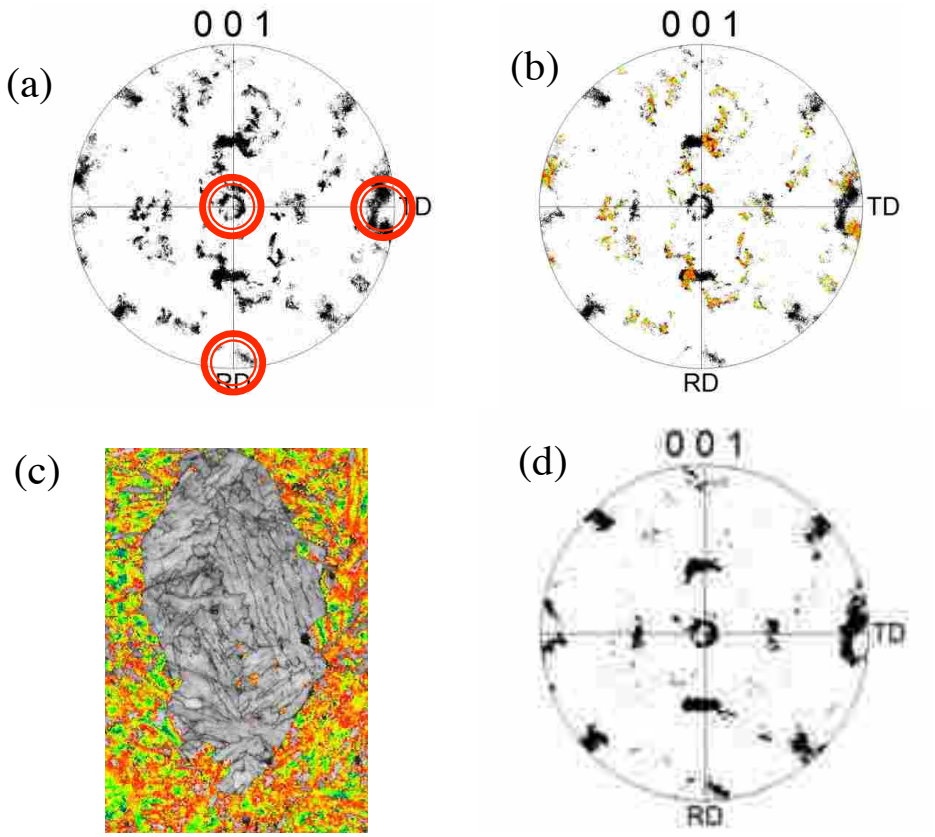

Figure 3-7: (a) Rotated PF of the cropped region. (b) Eliminated the outliers in rotated PF (c) Eliminated outliers in IQ map, the non-highlighted part is one prior austenite grain. (d) PF of the reconstructed prior austenite grain (after eliminating the outliers)

It should be noted that the Bain zones in Figure 3-7d are incomplete compared to the ideal PF. This indicates that not all of variants were operative during the transformation. Bhadeshia [44] reported similar results about bainite transformation under externally applied stress. This illustrates that the axial-force applied during FSW somehow influences the deformation occurring during transformation.

The PAG reconstruction process meets some difficulties in the higher heat input welds. The primary microstructure is not only upper bainite, but also with some polygonal/allotriomorphic ferrites. Polygonal/allotriomorphic ferrites nucleate at austenite grain boundaries and obey K-S orientations. However, their growth may extend to adjacent austenite

grain with a random orientation. [37] Therefore, the transformed polygonal/allotriomorphic grain boundary ferrites are assigned to the appropriate parent austenite grain based on the orientation direction of their nucleation and growth.

By repeating the procedures described above, a map of the PAGs can be reconstructed as shown in Figure 3-8b. Although some PAG boundaries are clearly visible in Figure 3-8a, it is impossible to reconstruct the PAGs map like Figure 3-8b from direct observations.

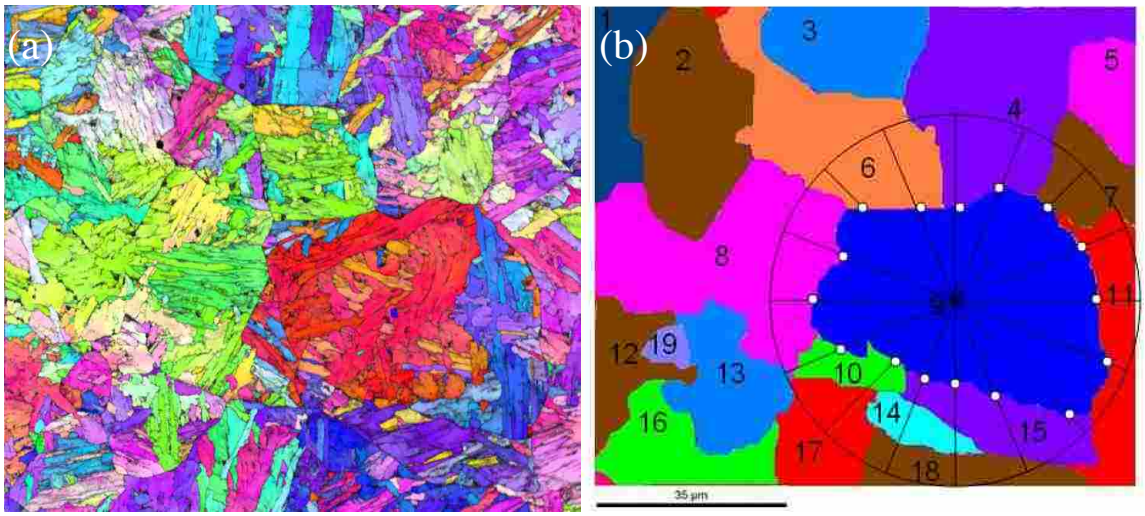

Figure 3-8: (a) IPF of the nugget center. (b) Reconstructed map of prior austenite grains in FSW nugget center, the number in the figure shows the individual austenite grains. The circle shows the new method to measure the PAG size, where the white solid circles show the interception of the circle with the PAG boundary.

The approach used to measure the prior austenite grain size will be described below. Traditional ASME intercept or planimetric methods are not suitable to use due to inadequate numbers of PAGs in the reconstruction map. A new method to measure the PAG size is developed. The schematic diagram is shown in Figure 3-8b. First, an 80mm-diameter circle is drawn on a transparency. The circle is equally divided into 16 parts by 8 diameters. Second, the

circle is placed on the top of each prior austenite grain and the intercepted length on each diameter is measured. The average value of eight measurements is the grain size of a PAG.

This new method to acquire grain size is good to measure the large grain size in the image with limited number grains. However, there are some limitations. For equiaxed grain, the average grain size is not sensitive to the placement of the circle center. However, for elongated grain, such as the grain six in Figure 3-8b, average grain size is very sensitive to the location of center. The error of measurement could be up to a 50-80% if the center of circle is placed closed to the edge of the grain. In order to get accurate measurement, there is at least one diameter of the circle across the longest axis of the elongate grain.

3.3.2 A Quantitative Approach to Bainite Packet Size Measurement

In this section, a quantitative approach to bainite packet size measurement is discussed. It is well-known the cleavage fracture resistance of bainitic microstructures is closely related to both PAGs and bainite packets since only high-angle bainite packet boundaries can efficiently stop the propagation of brittle cleavage microcracks. [53] So it is worth acquiring quantitative data of bainite packet size in FSW NC.

A bainite packet is composed of an aggregation of low-misorientation bainitic laths which have common crystallographic orientation. In the development of a bainite packet, new laths are frequently nucleated near the tips of laths. The formation of a bainite packet ceases when it conflicts with other packets. Bainite packet boundaries are defined as the high angle boundary. [44] Therefore, neighboring laths which belong to different bainite packets have the misorientation angle higher than 15°.

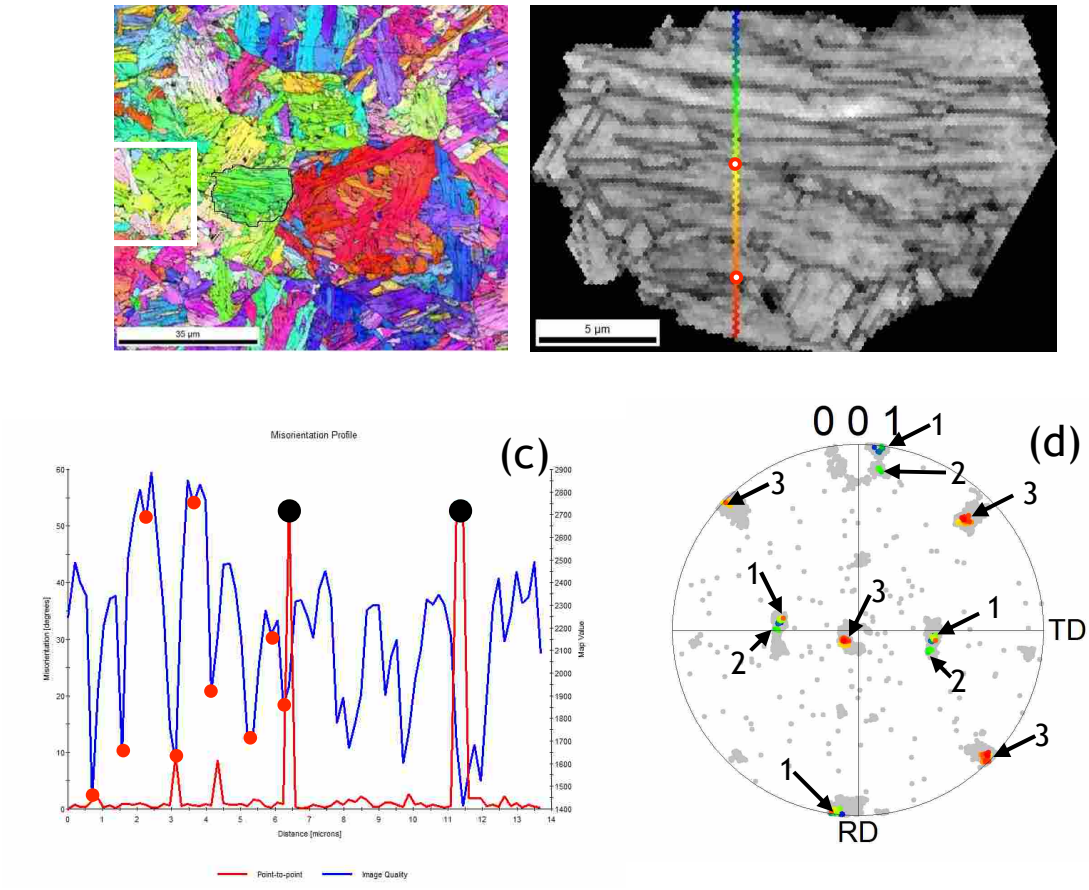

Figure 3-9: (a) IPF of the FSW NC, white space shows the irregular cropped region. (b) IQ map with the trace line across it. (c) Misorientation map is in red, high peaks show in black solid circles. IQ curve is in blue, red solid circles show the lower peak quantities. (d) PF, the variants are indicated by numbers

To illustrate the procedures of bainite packet size measurement, the cropped region shown in Figure 3-9a is used. Upon visual inspection of Figure 3-9b, it appears that this region may consist of one bainite packet. However, when a trace line is drawn across this "packet" as shown in Figure 3-9b, the misorientation plot of this region indicates more than one packet existed. The misorientation curve (red) reveals two peaks which have misorientation angles higher than 15°. According to bainite packet definition described in the preceding paragraph, it indicates three packets existed within this cropped region. Two red circles on the trace line in Figure 3-9b correspond to the positions of two peaks in the misorientation curve (red). These

reveal the bainite packet boundaries. The bainite packet size is measured as the distance between the misorientation angles higher than 15º.

The pole figure of the cropped region (in Figure 3-9d) provides additional evidence of three packets. The PF of this region is rotated to the reference position for ease of analysis. The blue, green and red dots are the corresponding variants along the trace line. It is obvious that there are three different variants representing different bainite packets. The variants are indicated by number. The variants are located on two primary Bain zones belonging to the same prior austenite grain.

3.3.3 Bainite Lath Size Measurement

Bainite lath size is determined from an image quality map and IQ value curve. In the IQ map, grain or lath boundaries have lower IQ value. [54] Therefore, bainite lath size is measured by plotting image quality along a trace line perpendicular to the lath boundary. The same cropped region shown in Figure 3-9b is used to illustrate. The IQ curve (blue) along the trace line is plotted in Figure 3-9c along with misorientation curve. Lath spacing is the distance between lower peaks of these quantities.

TEM was used to evaluate the accuracy of the bainite lath measurement taken by OIM™ .

Table 3-2 shows the comparison of lath measurement acquired by OIM™ and TEM. The lath measured by TEM ranges from 0.5-1.1μm. The measurements made by OIM™ are from 0.4 to 1.2μm. The average lath sizes acquired by OIM™ and TEM are differed by only a maximum of 2%.

Table 3-2: Comparison of measurement taken by OIM™ and TEM

	Measured by OIM™	*Measured by TEM*
Range	0.4~1.2 μm	0.35-1.15 μm
Average	0.86 μm	0.84 μm

3.4 Results and Discussions

3.4.1 Quantitative Data Collected by Using New Approaches

Quantitative measurements of post weld microstructures are acquired in FSW nugget center (NC) at four different heat inputs. PAG, bainite lath and packet sizes are measured using the approach described in the previous sections. The measurements were made at eight locations as illustrated in Figure 3-10 at each parameter to acquire the statistic data of bainite lath and packet size. The quantitative data acquired are summarized in Table 3-3.

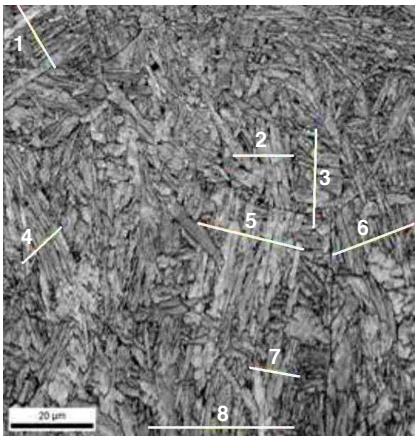

Figure 3-10: Measurement of bainite packet and lath sizes are taken at multiple locations in the FSW NC

Table 3-3: Quantitative data of microstructures in the FSW NC

Rotation Speed (rpm)	*Welding Speed (ipm)*	*Heat Input (J/mm)*	*Bainite Lath d (μm)*	*Bainite Packet Size w (μm)*	*PAG (μm)*	*Bainite Lath/Packet (d/w) Ratio*	*Bainite Packet Size w/PAG*
300	203.2	1308	0.653	2.754	10.234	1:4.22	1:3.72
600	203.2	1538	0.686	2.967	26.907	1:4.33	1:9.07
300	50.8	3329	0.703	3.137	30.400	1:4.46	1:9.69
600	50.8	4272	0.913	4.171	49.950	1:4.57	1:11.98

3.4.2 Heat Input Effects on Post-Weld Structures

3.4.2.1 Effect of Heat Input on Microstructures in the NC

In this section, some consideration will be given to post-weld microstructural changes at different heat inputs. Figure 3-11 compares the microstructures within the nugget center (NC) at various heat inputs and the base metal microstructure. The tool rotation speed (rpm) and welding speed (mm/min) are noted in the upper right hand corner of each micrograph. Heat inputs are noted in the bottom right-hand corners.

From OIM™ images, several microstructural characteristics can be observed. There is no evidence of base metal (BM) microstructures shown in Figure 3-11(a)-(d). The equiaxed grains in BM have completely transformed to upper lath bainite with some polygonal and allotriomorphic grain boundary ferrite. This indicates that the BM has reached a peak temperature in excess of the A_3, even at the lowest heat input 1308J/mm. In addition, grain and lath size in the NC is finer than BM. The refined grains may be due to recrystallization occurring or faster cooling associate with FSW process. In addition, prior austenite grain boundaries can be clearly observed at lower heat input. At higher heat input, the prior austenite grain boundaries are discontinuous.

At different heat inputs, the microstructural features are different. When heat input is sufficiently low, the microstructure is predominantly upper lath bainite, as shown in Figure 3-11a. With increasing heat input, two kinds of microstructures are formed in Figure 3-11b and c, lath bainite and some polygonal ferrite are transformed. When the heat input reaches 4272J/mm, the predominant microstructures in Figure 3-11d are upper bainite with some polygonal ferrite and allotriomorphic grain boundary ferrite.

Although lath bainite is the predominate microstructure in the NC over the range of parameters varied, the shape of bainite is different. The bainite structures are more parallel at lower heat input, and more irregular at high heat input. Bainite lath boundaries are curved as shown in Figure 3-11d, indicating more plastic deformation is generated at higher heat input which produced more deformed lath bainite.

Several reasons may contribute to the different morphologies at various heat input. It is known that the difference in the ferrite morphology in high strength steel weld is owing to the difference in heat input. Heat input controls cooling rate in the weld, i.e. an increase in heat input results in slower the cooling rates. Cooling rate plays the decisive role in determining weld microstructure. At slower cooling rates, the polygonal and allotriomorphic grain boundary ferrites start to form. At lower heat input, the intermediate transformation product- upper bainite dominates.

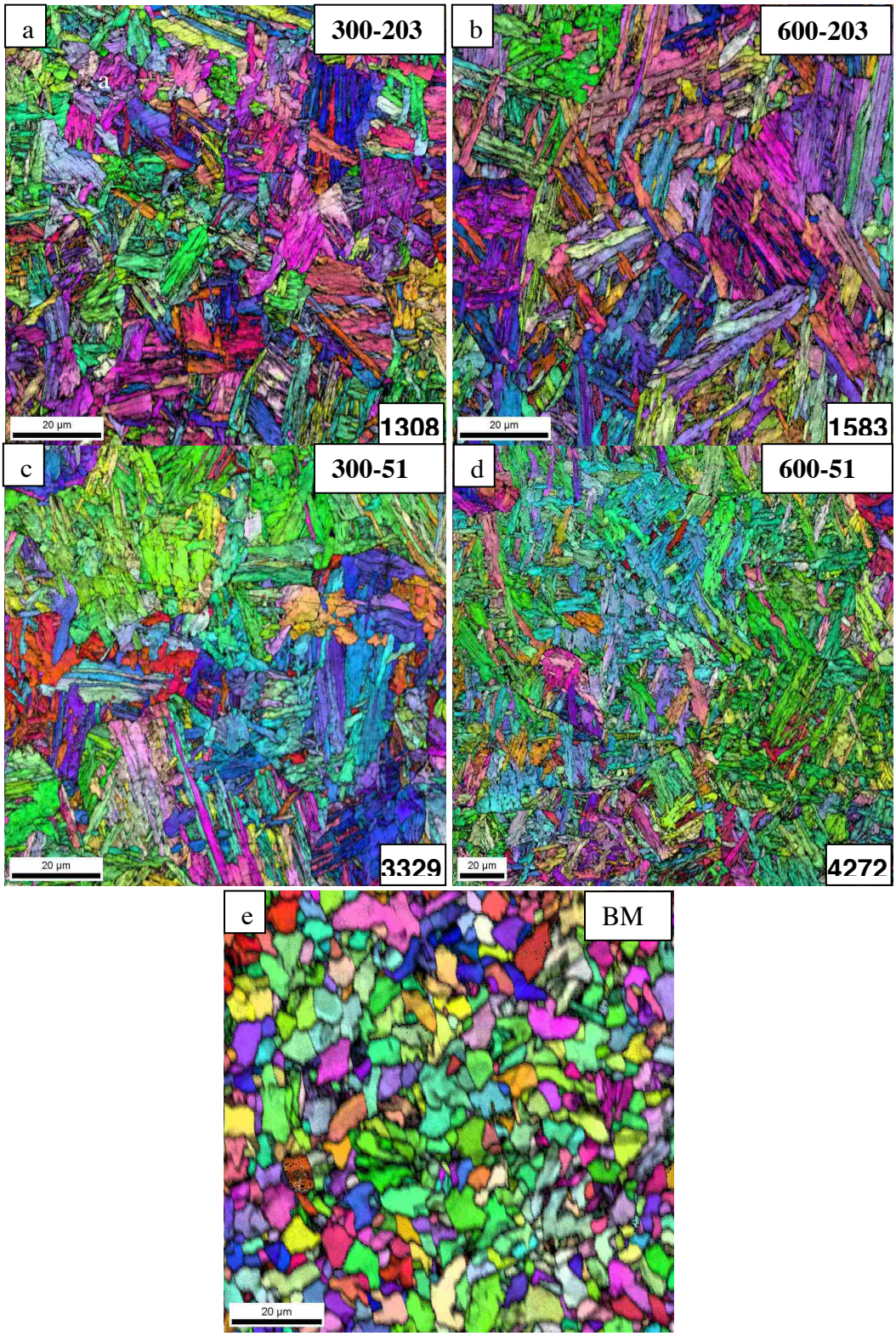

Figure 3-11: (a)-(d) Microstructures of weld nugget centre (NC) at various heat inputs, (e) base metal (BM)

3.4.2.2 Quantitative Microstructural Features in the NC

Based on the quantitative data acquired in Table 3-3, PAG size, bainite lath (d) and packet size (w) increase by 388%, 31% and 51% respectively, as heat input increases by 227%. Table 3-3 also summaries the ratio of bainite lath to packet size over a range of heat inputs investigated in this study. They are 1:4.22, 1:4.33, 1:4.46 and 1:4.57. The ratios have slight change. This indicates bainite lath and packet size increases with increasing heat input simultaneously.

Bainite lath/packet size and PAG size are plotted versus heat input as shown in Figure 3-12a-c. From the plots, bainite lath (d), bainite packet (w) and PAG size exhibit increasing trend with increasing heat input. In addition, bainite lath/packet size and PAG size display linear relationships with changing heat input (H.I). Figure 3-12 also shows the relationship between the prior austenite grain size and bainite packet size (w), as well as PAG size with bainite lath size (d) in the FSW HSLA 65 NC. Bainite lath (d) and packet (w) sizes increase linearly with increasing prior austenite grain size (PAG).

Several reasons can be attributed to these correlations. First, higher heat input produces higher peak temperature which will coarsen PAGs size. [38] Second, slower cooling rate associated with higher heat input provides longer time within austenite temperature range. [36] So higher heat input will enhance the formation of coarser prior austenite grains in the weld metal zone. It is well-known that prior austenite grain size plays an important role on the transformed microstructures, i.e., larger PAG will transform to coarser microstructures. During the bainite transformation, it involves compositional changes which require the diffusion of carbon. At higher heat input, it induces higher diffusion rate which causes longer carbon

diffusion length per unit time. Combined with higher peak temperature and slower cooling rate, it results in larger bainite lath and packet sizes in the weld nugget center.

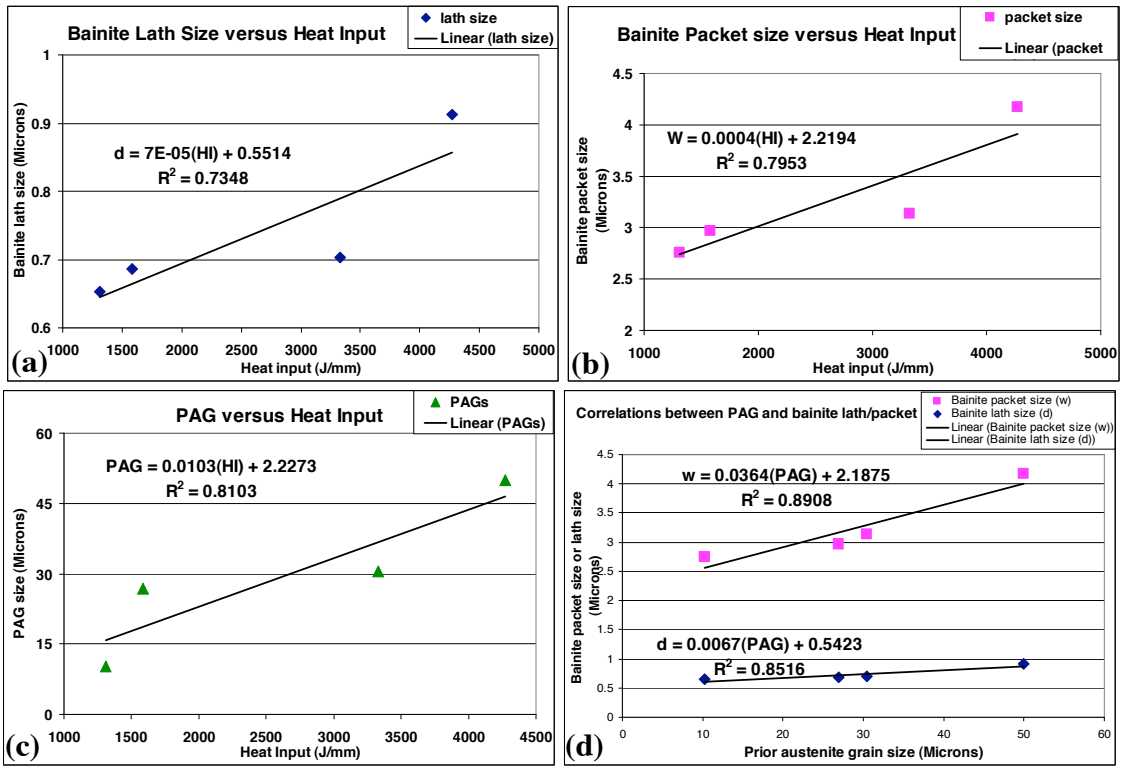

Figure 3-12: (a) Bainite lath size (b) bainite packet size (c) PAG size varies with changing heat input (d) bainite lath/packet size versus prior austenite grain size

3.4.3 Effect of Heat Input on Mechanical Properties in the NC

The tensile properties of the FSW NC are summarized in Table 3-4. Both yield strength (YS) and ultimate tensile strength (UTS) exceed the base metal minimum at all hat inputs. Tensile properties are plotted versus heat input as shown in Figure 3-13(a) and (b). YS and UTS in the NC exhibit linear relationships with heat input. YS shows linear relationships with bainite lath/packet size. The authors think R^2 values can be improved if more microstructural data at different heat input can be acquired.

Table 3-4: Tensile properties and hardness in the FSW NC

Rotation Speed (rpm)	*Welding Speed (ipm)*	*Heat Input (J/mm)*	*YS (ksi)*	*UTS (ksi)*
300	203.2	1308	85.9	104
600	203.2	1583	82.1	100.4
300	50.8	3329	80.0	99.8
600	50.8	4272	76.3	98.5
Base Metal			65	78

It is well-known that yield strength at room temperature depends on grain size according to the Hall-Petch relation, i.e. $YS = \sigma_0 + k_y d^{-1/2}$, where YS is the yield stress (in MPa), σ_0 is a constant, k_y is a constant representing the grain boundary as an obstacle to slip across the grain boundaries, and d is the grain size (in mm). In this case, yield stress dependant on bainite lath (d), packet size (w) and PAG size is shown in Figure 3-13c. The linear behavior follows a Hall-Petch type relationship too.

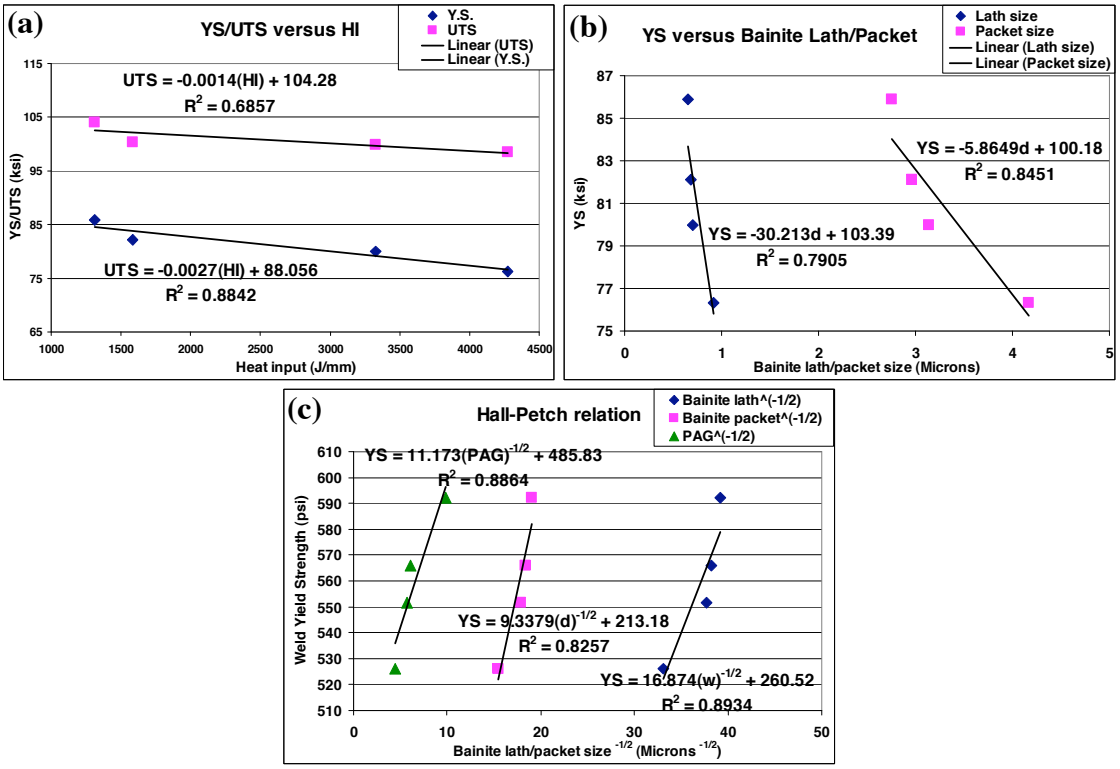

Figure 3-13: (a) YS/UTS versus HI (b) YS versus bainite lath/packet sizes (c) Hall-Petch relations between YS and bainite lath/packet in the FSW NC

These phenomena in mechanical properties can be explained by the results of microstructural observation. Mechanical properties of steels are strongly dependent on the microstructure. Microstructural changes in the weld nugget (NC) are associated with the peak temperature and cooling rates, which in turn depend on the weld heat input.

NC in wide range parameters are characterized primarily as bainite with some polygonal ferrite. More bainite is produced at lower heat input, and more polygonal ferrites are produced at higher heat input. Since bainite has higher strength than polygonal ferrite, lower heat input weld has higher yield property. In addition, the linear Hall-Petch relations shown in Figure 3-13c illustrates that YS highly depends on bainite lath/packet sizes and PAG size. Finer bainite lath/packet sizes and PAG size are, higher tensile properties are.

3.5 Conclusions

In this study, the new approaches have been developed to acquire quantitative microstructural data in HSLA type steels. These quantitative data enable to establish the correlations between microstructures, mechanical properties and process variables in the FSW nugget center. From the analysis, the following conclusions can be made:

- A new approach has been developed to acquire quantitative microstructural data via OIM™ .
    - In this study, it is specifically used to measure bainite lath and packet sizes.
    - A new approach is developed to reconstruct prior austenite grain (PAG) structure from room temperature ferrite.

- With the new approach, quantitative post-weld microstructural data in HSLA type steels is easily to obtain now.

- Quantitative microstructural data have been used to develop correlations between microstructures, mechanical properties and FSW process variables in the FSW weld nugget center.
  - Bainite lath/packet size exhibits linear relationships with heat input.
  - Prior austenite grain size show linear relationship with heat input.
  - Bainite packet and lath sizes increase linearly as the PAGs size increases.
  - Tensile properties display power relationships with heat input.
  - YS is highly dependent on bainite lath/packet size and PAG size. They follow Hall-Petch relation.
- These correlations can be used to determine FSW weld parameters for desired mechanical properties welds.

REFERENCES

1 Dawes, C.J., Thomas, W.M., *TWI Bull*. 6 (1995), 138

2 James, M., Mahoney, M., *Proceedings of the First International Symposium on Friction Stir Welding,* Thousand Oaks, CA, USA, June 14-16, 1999

3 Mohoney, M.V., Rhodes C.G., Flintoff, J.G., Spurling, R.A., Bingel W.H., *Metall Mater Trans* 1998;38:703

4 Rhodes, C.G., Mohoney, M.V., Bingel W.H., Spurling R.A., Bampton C.C., *Scripta Mater*, 1997;36:69

5 Jata, K.V., Sankaran, K.K., Ruschau, J.J., *Metall Mater Trans*, 2000;31A:2181

6 Reynolds, A.P., Lockwood, W.D., Seidel, T.U., *Mater. Sci. Forum,* 331–337 (2000), 1719–1724

7 Thomas, W.M., et al., *International Patent Application Number PCT/GB92/02203 and GB Application Number 9125978.8*, 1991

8 Juhas, M.C., Viswanathan, G.B., Fraser, H.L., *Proceedings of the Second Symposium on Friction Stir Welding*, Gothernburgm Sweden, June 2000

9 Park, H.S., Kimura, T.K., Murakami, T., Nagano, Y., Nakata, K., Ushio, M., "Microstructure and Mechanical Properties of Friction Stri Welds of 60%Cu-40%Zn Copper Alloy." *Mater, Sci. Eng. A* 371 (2004), 160-169

10 Lee, W.B., Jung, S.B., "The Joint Properties of Copper by Friction Stir Welding." *Mater. Lett*. 58(2004), 1041-1046

11 Cui, L., Fujii, H., Tsuji, N., Nakata, K., Nogi, K., Ikeda, R., Matsushita, M., "Transformation in Stir Zone of Friction Stir Welded Carbon Steels with Different Carbon Contents." *ISIJ International*, Vol. 47, 2007, No. 2, 299-306

12 Ueji, R., Fujii, H., Cui, L., Nishioka, A., Kunishige, K., Nogi, K., "Friction Stir Welding of Ultrafine Plain Low-carbon Steel Formed by the Martensite Process." *Materials Science & Engineering A*, 423, 2006, 324-330

13 Fujii, H., Cui, L., Tsuji, N., Maeda, M., Nakata, K., Nogi, K., "Friction Stir Welding of Carbon Steels." *Materials Science and Engineering A*, 429, 2006, 50-57

14 Posada, M., Deloach, J., Reynolds, A.P., Skinner, M., Halpin, J.P., "Friction Stir Weld Evaluation of HH-36 and Stainless Steel Weldment." *Friction Stir Welding and Processing*, Indianapolis, IN, USA, 4-8 Nov. 2001, 159-171

15 Sato, Y.S., Nelson, T.W., Sterling, C.J., Steel, R.J., Pettersson, C.O., "Microstructure and Mechanical Properties of Friction Stir Welded SAF 2507 Super Duplex Stainless Steel." *Materials Science & Engineering A*, 397, 2005, 376-384

16 Sampath, K., "An Understanding of HSLA-65 Plate Steels." *Journal of Materials Engineering and Performance*, Volume 15(1) February 2006, 32-40

17 Konkol, P.J., Mathers, J.A., Johnson, R., Pickerns, J.R., "Friction Stir Welding of HSLA-65 Steel for Shipbuilding", Journal of Ship Production, Vol. 19, No. 3, August 2003, 159-164

18 Ozekcin, A., Jin, H.W., Koo, J.Y., Bangaru, N.V., Ayer, R., "A Microstructural Study of Friction Stir Welded Joints of Carbon Steels." *International Journal of Offshore and Polar Engineering*, Vol. 14, No. 4, December 2004

19 Nelson, T.W., Su, J.Q., Steel, R.J., "Friction Stir Welding of Ferritic Steels." *Proceedings of ISOPE-2004: Fourteenth (2004) International Offshore and Polar Engineering Conference*. 2004

20 Pao, P.S., Fonda, R.W., Jones, H.N., Feng, C.R., Moon, D.W., "Friction Stir Welding of HSLA-65 Steel." *Friction Stir Welding and Processing IV*, 243-251

21 Posada, M., DeLoach, J., Reynolds, A.P., Fonda, R., Halpin, J., "Evaluation of Friction Stir Welded HSLA-65." *4th International Friction Stir Welding Symposium*, Park City UT, USA

22 Querin, J.A., Davis, A.M., Schneider, J.A., "Effect of Processing Parameters on Microstructure of the FSW Nugget." *Friction Stir Welding and Processing IV*, 185-192

23 Rodrigues, D.M., Loureiro, A., Leitao, C., Leal, R.M., Chaparro, B.M., Vilaca, P., "Influence of Friction Stir Welding Parameters on the Microstructural and Mechanical Properties of AA 6016-T4 Thin Welds", *Materials and Design*, 30 (2009), 1913-1921

24 Afrin, N., Chen, D.L., Cao, X., Jahazi, M., "Microstructure and Tensile Properties of Friction Stir Welded AZ31B Magnesium Alloy", *Materials Science and Engineering A*, 472, 2008, 179-186

25 Cao, X., Jahazi, M., "Effect of Welding Speed on the Quality of Friction Stir Welded Butt Joints of a Magnesium Alloy, *Material and Design*, 30 (2009), 2033-2042

26 Cui, S., Chen, Z.W., "Effects of Rotation Speed and Welding Speed on Material Flow and Stir Zone Formation during FSW/P." *Friction Stir Welding and Processing V, TMS Annual Conference*, 2009, 125-133

27 Adam, L., Pilchak, Z., Li, T., Fisher, J.J., Reynolds, A.P., Juhas, M.C., Williams, J.C., "The Relationship between Friction Stir Process (FSP) Parameters and Microstructure in Investment Cast Ti-6Al-4V", *Friction Stir Welding and Processing IV*, 2007, 419-428

28 Gunaraj, V., Murugan, N., "Prediction and Comparison of the Area of the Heat-affected Zone for the Bead-on-plate and Bead-on-joint in Submerged Arc Welding of Pipes." *Journal of Materials Processing Technology*, 95 (1999), 246-261

29 Quan, Y.J., Chen, Z.H., Gong, X.S., Yu, Z.H., "Effects of Heat Input on Microstructure and Tensile Properties of Laser Welded Magnesium Alloy AZ31", *Materials Characterization*, 59, 2008, 1491-1497

30 Nelson, T.W., Anderson, S.J., Segrera, D.J., "Friction Stir Welding of X-65 Steel." *Friction Stir Welding and Processing IV*, 269-277

31 Reynolds, A.P., "Microstructure Development in Aluminum Alloy Friction Stir Welds." *Friction Stir Welding Processing*, Chapter 4, 51-70

32 Arbegast, W., "Hot Deformation of Aluminum Alloys III." *TMS*, 2003, Warrendale, PA, 313-327

33 Sanders, D., Edwards, P., Grant, G., Ramulu, M., Reynolds, A., "Superplastically Formed Friction Stir Welded Tailored Aluminum and Titanium Blanks for Aerospace Applications", *6th EuroSPF Conference*, 2008, Carcassonne: France

34 Balasubramanian, N., Gattu, B., Mishra, R.S., *Science and Technology of Welding and Joining*, Vol. 14, No. 2, 2009, 141-145

35 Pew, J.W., Nelson, T.W., Sorensen, C.D., "Development of a Torque-based Weld Power Model for Friction Stir Welding." *Friction Stir Welding and Processing IV*, 2007, 73-82

36 Patchett, B.M., Bringas, J.E., Thomas, R.D., *The Metals Blue Book*, 19

37 Grong, Ø., *Metallurgical Modeling of Welding*, 406-450

38 Reed-Hill, R.E., Abbaschian, R., *Physical Metallurgy Principles*, 642-644

39 Khandkar, M.Z.H., Khan, J.A., Reynolds, A.P., *Sci. Technol. Weld. Join.*, Vol 8 (No. 3), June 1, 2003, 165-174

40 Wei, L.Y., Nelson, T.W., "Characterization of Microstructures and Transformation Behavior in Friction Stir Welded HSLA-65." *8th International Conference on Trends in Welding Research,* 2008, Pine Mountain, GA, USA

41 Wei, L.Y., Nelson, T.W., "Correlate Microstructures and Process Variables in FSW HSLA-65 Steel"

42 Rajasekhar, A., Reddy, G.M., Mohandas, T., Murti, V.S.R., "Influence of Austenitizing Temperature on Microstructure and Mechanical Properties of AISI 431 Martensitic Stainless Steel Electron Beam Welds", *Materials and Design, 30 (2009),* 1612-1624

43 Lambert-Perlade, A., Gourgues, A.F., Pineau, A., "Austenite to Bainite Phase Transformation in the Heat-Affected Zone of a High Strength Low Alloy Steel." *Acta Materialia,* 52 (2004), 2337-2348

44 Bhadeshia, H.K.D.H., Christian, J.W., "Bainite in Steels." *Metallurgical Transactions* A, Volume 21A, April, 1990, 206-215, 767-797

45 Chen, Z., Shan, Z.W., Wu, N.Q., Sikka, V.K., Hua, M.J., Mao, S.X., "Fine Carbide-Strengthened 3Cr-3WVTa, Bainitic Steel", *Metallurgical and Materials Transactions, A,* Volume 35A, April 2004, 281-1288

46 Bangaru, N.V., Fairchild, D.P., Macia, M.L., Koo, J.Y., Ozekcin, A., "Microstructural Aspects of High Strength Pipeline Girth Welds", *4th International conference on Pipeline Technology,* Ostend, Belgium, 2004

47 Nelson, T.W., Wei, L.Y., Abbasi, M., "Quantifying Post-Weld Microstructures in FSW HSLA-65", *TMS Annual Conference 2009*, San Francisco, CA, USA, Feb 15-19, 2009

48 Decocker, R., Kestens, L., Petrov, P., Houbaert, Y., "Revealing a Parent Phase Structure after Transformation Based on Crystallographic Relations", *Trans Tech Publications,* Switzerland, THERMEC' 2003, 3751-3756

49 Cayron, C., Artaud, B., Briottet, L., "Reconstruction of Parent Grains from EBSD Data", *Materials Characterization*, 57, 2006, 386-401

50 He, Y., Jonas, J.J., "Representation of Orientation Relationships in Rodrigues-Frank Space for any two Classes of Lattice", *Journal of Applied Crystallography,* 2007, 40, 559-569

51 He, Y., Godet, S., Jonas, J.J., "Representation of Misorientations in Rodrigues-Frank Space: Application to the Bain, Kurdjumov-Sachs, Nishiyama-Wassermann and Pitsch Orientation Relationships in the Gibeon Meteorite", *Acta Materialia,* 53, 2005, 1179-1190

52 Ryder, P.L., Pitsch, W., Mehl, R.F., *Acta Metall.,* 1967, 15, 1431-1440

53 Pickering, F.B., "The Structure and Properties of Bainite in Steels", *Proceedings of the Transformation and Hardenability in Steels*, Ann Harbor, MI, Climax Molybdenum, 1967, 109

54 Nowell, M., Witt, R., True, B., "EBSD Sample Preparation Techniques, Tips, and Tricks", *EDAX-TSL Manual*, 2006